Journal of Materials Science and Chemical Engineering, 2023, 11, 48-74
https://www.scirp.org/journal/msce
ISSN Online: 2327-6053
ISSN Print: 2327-6045

# CI Acid Orange 52 Dye Removal Using Natural and Formulated Clay-Lime Materials: Isotherm, Kinetic and Thermodynamic Studies

**Fumba Gaston[1], Essomba Jean Serge[1,2], Ankoro Naphtali Odogu[3], Kouotou Daouda[1], Bélibi Bélibi Placide Désiré[1], Ndi Julius Nsami[1*], Ketcha Mbadcam Joseph[1]**

[1]Laboratory of Applied Physical and Analytical Chemistry, Department of Inorganic Chemistry, Faculty of Science, University of Yaoundé I, Yaoundé ,Cameroon
[2]Inorganic and Physical Chemistry Lab, CSIR-Central Leather Research Institute, Chennai, India
[3]Department of Chemistry, Faculty of Science, University of Buea, Buea, Cameroon
Email: *bigpielo2002@yahoo.com

**How to cite this paper:** Gaston, F., Serge, E.J., Odogu, A.N., Daouda, K., Désiré, B.B.P., Nsami, N.J. and Joseph, K.M. (2023) CI Acid Orange 52 Dye Removal Using Natural and Formulated Clay-Lime Materials: Isotherm, Kinetic and Thermodynamic Studies. *Journal of Materials Science and Chemical Engineering*, **11**, 48-74.
https://doi.org/10.4236/msce.2023.1111005

**Received:** September 13, 2023
**Accepted:** November 27, 2023
**Published:** November 30, 2023



## Abstract

The main objective of the study is to improve the removal efficiency of Ourlago-kaolin (Kao), sodium montmorillonite (Na-MMT), and two formulated clay-lime (F13 and F23) towards CI Acid Orange 52 dye (AO52). F13 and F23 were obtained by chemical stabilization through thermal treatment at 300°C. Fourier Transform Infrared spectra showed different surface functional groups on the clay materials, X-ray diffraction patterns revealed the raw materials contain many crystalline phases, scanning electron microscopy micrographs showed the variation of the layered structures of different clay materials, energy dispersive X-Ray analysis micrographs revealed compositional information and thermogravimetric-differential scanning calorimetry curves indicated the higher weight loss of 11.26% and 11.38% were observed for F13 and F23 respectively. BET surface area analyzed gave 133.0071 $m^2 \cdot g^{-1}$ for F13 and 132.34803 $m^2 \cdot g^{-1}$ for F23. The optimum pH value was 2.0 for Kao and Na-MMT. The adsorption experiments indicated that F13 and F23 have the maximum uptake abilities of 7.8740 and 3.1645 $mg \cdot g^{-1}$, respectively, compared to Kao (0.8761 $mg \cdot g^{-1}$) and Na-MMT (2.6178 $mg \cdot g^{-1}$). The pseudo-second-order model well described the adsorption kinetic model of AO52 dye onto the overall samples; Langmuir and Freundlich's isotherms appropriately described the uptake mechanism. The positive values of $\Delta G^{\circ}$ and negative value $\Delta H^{\circ}$ indicated that the adsorption process was spontaneous and endothermic for Na-MMT, and non-spontaneous and exothermic for Kao, F13, and F23 because of their positive values of $\Delta G^{\circ}$ and negative value of $\Delta H^{\circ}$. The modified clays have higher adsorption capacities and better life cycles com-

pared hence opening new avenues for efficient wastewater treatment.

## Keywords

Ourlago-Kaolin, Sodium Montmorillonite, Formulated Clay Lime, Adsorption, Acid Dye, Thermodynamic

## 1. Introduction

The demographic boom and the advent of industries have created an enormous demand for water, the quality of which must be safeguarded [1]. Several industries like paper, soft goods, skin, and cosmetics employ dyestuff to tint inherent goods and also deplete a great quantity of water. As a consequence, they discharge large quantities of dye-containing wastewater [2]. To date, more than $10^4$ dyes are accessible in the wholesale, with an annual production of more than $7 \times 10^5$ tons known [3]. Meanwhile, around 10% - 20% of the pigments are rejected during manufacturing operations, which induces the discharge of huge quantities of colored effluents [4]. Color is one of the easily recognizable pollutants in wastewater because even at very low concentrations, less than 1ppm in water, certain dyes are visible and non-desirable [5]. Dyes are organic substances that are dangerous for humans because they have been found to be toxic and carcinogenic agents. Like many other acid dyes, CI Acid Orange 52 induces human health problems such as skin problems and eye irritation. Hence, it is necessary to eliminate colors in water to prevent any contamination.

Several techniques, including physical, chemical, and biological methods have been developed to remove synthetic dyes from aqueous solutions. These comprise the filtration membrane, flocculation, jellification, microbiologic or enzymic dissolution, innovative autolysis, and adsorption [6]. Among the overall colored wastewater treatment techniques that exist, adsorption stands out as a highly competent technology for the removal of pollutants from wastewater due to its simplicity, cost-effectiveness, and efficiency. In addition, it is an eco-friendly technique [7].

Many investigators have used various less expensive alternative adsorbents to bon-activated, orange peels, banana peels, kola nut and coconut shells, fly ash, and clay minerals have been much more quoted during the last decade [6]. Among them, clay minerals are frequently used in environment curing because of their structural and surface properties, such as the fineness of the particles, the degree of plasticity, and the large specific surface area [8] [9]. At a certain degree of purity, natural clays are used to purify water. However, in order to improve their adsorption ability; they are physically or chemically modified to increase their porosity as well as their specific surface area. The activated and modified clay materials are often more efficient in the adsorption process than the native

clay. This present study describes an investigation of differences in removal properties of acid dye in an aqueous solution between four adsorbents namely Ourlago-kaolin (Kao), sodium montmorillonite (Na-MMT) and two formulated clay-lime (F13 and F23). The chemical and thermal properties of adsorbents are also examined in detail.

## 2. Equipment and Standard Procedure

### 2.1. Equipment

In order to show the adsorption capacity of the clay materials, an acid dye namely CI Acid Orange 52 (AO52) was chosen as a simple model which is an intensely colored compound used in dyeing and printing textiles. This dye was purchased from FlukaChemika, its heterocyclic aromatic chemical compound, its density is 1.28 g·cm$^{-3}$, its molecular formula is $C_{14}H_{14}N_3NaO_3S$ and its molecular mass of 327.34 g·mol$^{-1}$. Figure 1 gives the CI Acid Orange 52 dye structure.

#### Adsorbents Preparation

1) Purification of the natural clay materials

The natural clays used here were collected from Cameroon. The particle size less than 2 μm was obtained by purification of the raw clays. These raw samples were distributed in a graded sedimentation device and a few quantities of a dispersing agent namely dolaflux were added at a given time t according to the Stockes equation:

$$t = 191.5 \times \frac{x}{d^2} \quad [10]$$

where: $t$ (min) is the required time, $d$ (μm) is a particle diameter and $x$ (cm) is the depth that could be reached by the particle. The cation exchange capacity (CEC) of the raw materials was determined according to ASTM C837-09 standard and was found to be 11.2 meq/100g for Kao and 95.8 meq/100g for Ca-MMT.

2) Preparation of sodium montmorillonite (Na-MMT)

Purified calcium montmorillonite (Ca-MMT) was used as raw material in the preparation of Na-MMT. Ion exchange reaction using $Na_2CO_3$ was the key reaction according to the following procedure [11]: A suspension of 10 wt.% Ca-MMT in water was prepared and caused to swell with continuous stirring at room temperature. 1 h later, after adding a few quantities of $Na_2CO_3$, the suspension was agitated for 8 h at 80˚C using a stirring hot plate.

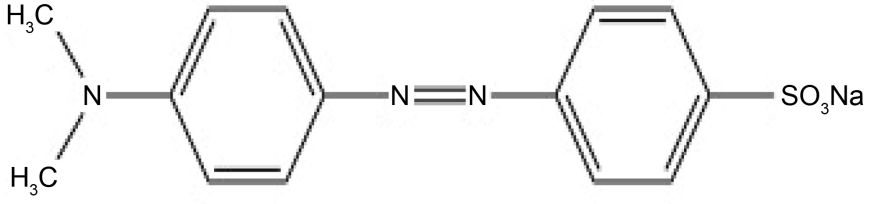


Figure 1. CI Acid Orange 52 dye structure.

3) Preparation of the formulated clay lime

To optimize the removal efficiency of CI Acid Orange 52 onto the two natural clay materials, the physical method was used to prepare the formulated clay lime mixture. Table 1 gives clay mineral components of the mineral mixture calcined at 300˚C for 90 min. The calcium hydroxide was used in this study as the principal source of calcium.

4) Preparation of CI Acid Orange 52 solution

Stock solution of CI Acid Orange 52 (200 $mg{\cdot}L^{-1}$) which is used as synthetic dye effluent called adsorbate for the present study was obtained by adding 0.200 g of acid dye taken within 1L volumetric flask with distilled water.

## 2.2. Standard Procedure

### 2.2.1. Material Characterization

Many techniques were used to characterize the different adsorbents. XRD of the raw materials is retrieved on an XG actinism diffractometer applying CuKα emission ($\lambda$ = 1.5418 Å) through 30,000 V/15mA with a scanning speed of $2^{\circ}{\cdot}min^{-1}$ and the $2\theta$ angle between 5˚ - 80˚. The FT-IR spectra are obtained from a spectrometer brand spectrum 100 (USA) in the central zone of (4000 - 400 $cm^{-1}$). The TG-DSC spectra are obtained from an apparatus in which the increase in the heating rate is from $1^{\circ}C{\cdot}min^{-1}$ at ambient temperature upper limit of 800˚C in atmospheric air. SEM coupled with EDX was performed on the JOEL JBN-5600 instrument. Brunauer-Emmett-Teller (BET) surface area of raw and modified clay materials was determined by micrometrics ASAP 2020 V3.00 H. Pore size distribution was calculated by the Barrett-Joyner-Halenda (BJH) method.

### 2.2.2. Batch Adsorption

The adsorption studies in batch mode were carried out using the 250 mL conical flasks (Kimax, USA) as batch reactors. To perform the kinetic study, eight 250 mL conical flasks each containing 0.1 g of adsorbent and 20 mL AO52 dye solution with a concentration of 10 $mg{\cdot}L^{-1}$, were stirred on a multistation shaker set at a speed of 250 rpm at ambient temperature (25˚C ± 2˚C) at different times 3, 5, 10, 15, 20, 25, 30 and 40 min. Adsorption isotherm studies were performed at AO52 concentrations varying from 4 - 12 mg/L. After the adsorption process, to determine the residual concentration, the filtrate was assayed using UV-visible spectrophotometer (Model-S23A) at the wavelength of the maximum adsorption of 465 nm. The Metrohm brand 744 pH meter was used to measure the pH of

**Table 1.** Different formulations of the mixtures calcined at 300˚C for 90 min.

| Constituent (%) | Calcined formulated clay lime at 300˚C | |
|---|---|---|
| | F13 | F23 |
| Calcium hydroxide ($Ca(OH)_2$) | 65 | 70 |
| Sodium montmorillonite (Na-MMT) | 20 | 15 |
| Ourlago-kaolin (Kao) | 15 | 15 |

AO52 dye solution. To study the influence of the pH of the AO52 solution, the solutions of HCl or NaOH (0.1 N) were used to adjust the pH of the initial solution of dye by varying from 2 - 12. The reactors contained 0.1 g sample and 20 mL of 10 mg·L$^{-1}$ AO52 dye that was reacted for a specific time at ambient temperature. The effect of temperature on the adsorption kinetics of AO52 dye was taken into account at variable temperatures 25˚C, 30˚C, 40˚C and 60˚C, 0.5 g of adsorbent was added in 100 mL of 10 mg/L of AO52 dye and brought to stirring for the equilibrium time of each adsorbent. The amount of AO52 dye adsorbed at equilibrium ($q_e$) and adsorption percentage (%$R$) of all the clay materials are calculated according to the equations below.

$$q_e = \frac{C_o - C_e}{m} \times V \tag{1}$$

$$\%R = \frac{C_o - C_e}{C_o} \times 100 \tag{2}$$

where $q_e$ (mg·g$^{-1}$) is the equilibrium amount of dye adsorbed, $C_o$ and $C_e$ are the initial and equilibrium AO52 dye concentrations respectively, $m$ (g) is the sample weight, $V$ is the dye solution volume (mL).

### 2.2.3. Kinetic Study

The kinetic models used to describe the adsorption kinetics of AO52 dye onto clay materials in aqueous solutions are given in Table 2.

### 2.2.4. Adsorption Isotherms

Langmuir and Freundlich isotherm models were used to describe the adsorption mechanism of AO52 dye as shown in Table 3.

**Table 2.** Pseudo-first-order and pseudo-second-order kinetic models.

| Kinetic models | Kinetic equation | Parameters | References |
|---|---|---|---|
| Pseudo-first-order | $\frac{dq}{dt} = k_{1,ads}(q_e - q_t)$<br>$\log(q_e - q_t) = \log q_e - \frac{k_{1,ads} \cdot t}{2.303}$ | $q_e$ (mg·g$^{-1}$)<br>$k_{1,ads}$ (min$^{-1}$) | [12] |
| Pseudo-second-order | $\frac{dq}{dt} = k_{2,ads}(q_e - q_t)^2$<br>$\frac{t}{q_t} = \frac{1}{k_{2,ads} q_e^2} + \frac{t}{q_e}$ | $k_{2,ads}$<br>(g·mg$^{-1}$·min$^{-1}$)<br>$q_e$ (mg·g$^{-1}$) | [13] |

**Table 3.** Langmuir and Freundlich isotherm models.

| Isotherm models | Isotherm equation | Parameters | References |
|---|---|---|---|
| Langmuir | $\frac{1}{q_e} = \frac{1}{q_{max}} + \frac{1}{K_L q_{max} C_e}$ | $q_{max}$ (mg·g$^{-1}$)<br>$K_L$ (L·mg$^{-1}$) | [14] |
| Freundlich | $\ln q_e = \ln K_f + \frac{1}{n} \ln C_e$ | $K_f$(mg·g$^{-1}$·min$^{-1}$) and $n$ | [15] |

The essential characteristic ($R_L$) of the Langmuir isotherm is defined by the following equation [16].

$$R_L = \frac{1}{1 + K_L C_o} \tag{3}$$

The nature of the adsorption process depends on the $R_L$ values: If $R_L > 1$: unfavorable;

$R_L = 1$: linear; $R_L \in ]0;1[$ : favourable and $R_L = 0$: irreversible.

#### 2.2.5. Thermodynamic Study

The thermodynamic constants such as Gibbs energy ($\Delta G^\circ$), enthalpy ($\Delta H^\circ$) and entropy ($\Delta S^\circ$) were calculated by using both the thermodynamics and Van't Hoff equations [17].

$$K_d = \frac{C_{ads}}{C_{solution}} \tag{4}$$

$$\Delta G^\circ = -RT \ln K_d \tag{5}$$

$$\ln K_d = \frac{\Delta S^\circ}{R} - \frac{\Delta H^\circ}{RT} \tag{6}$$

In which $R$ is the universal gas constant, $T$ is the temperature in (K), and $K_d$ is the partition measure, $C_{ads}$ is the concentration of the solute adsorbed on the samples in ($mg \cdot g^{-1}$) and $C_{solution}$ is the first measured initial concentration of the solute ($mg \cdot g^{-1}$).

## 3. Results and Discussion

### 3.1. Characterization

#### 3.1.1. FT-IR Spectroscopy Analysis of Clay Materials

**Figure 2** shows the FT-IR spectra of Kao (a), Na-MMT (b), F13 (c) and F23 (d) respectively. **Figure 2(a)** and **Figure 2(b)** were utilized to validate the formation of formulated clay lime mixtures F13 and F23. **Figure 2(a)** indicates that the absorption bands at 3694 and 3619.88 $cm^{-1}$ in the Ourlago-kaolin sample, were attributed to the intermediate layer hydroxyl (O-H) assemblage and the group at 3433.14 $cm^{-1}$ was assigned to the O-H bonds pointing in the layers of the tetrahedral sheets [18]. Absorption bands at 993.33 $cm^{-1}$ were related to the stretching Si-O bonds, whereas the absorption band at 523.28 $cm^{-1}$ characterized the Al-O-Si bond in kaolinite. The very low absorption band at 795.22 $cm^{-1}$ shows the presence of quartz in the clay materials.

As shown in **Figure 2(b)**, the characteristic bands of bending vibration bond Si-O of quartz appear at 524.75 $cm^{-1}$ and 644.75 $cm^{-1}$; 690.50 and 419.39 $cm^{-1}$ [19]. In this figure, the absorption band at 3696 $cm^{-1}$ can be attributed to the stretching vibration of the inner OH located on the edge of the layers. Absorption bands at 3619.87 and 1631.75 $cm^{-1}$ correspond to the O-H stretching vibration and bending vibration of $H_2O$ of sodium montmorillonite. The Si-O and Si-O-Si bonds can be attributed to the absorption bands at 996.16 $cm^{-1}$ and

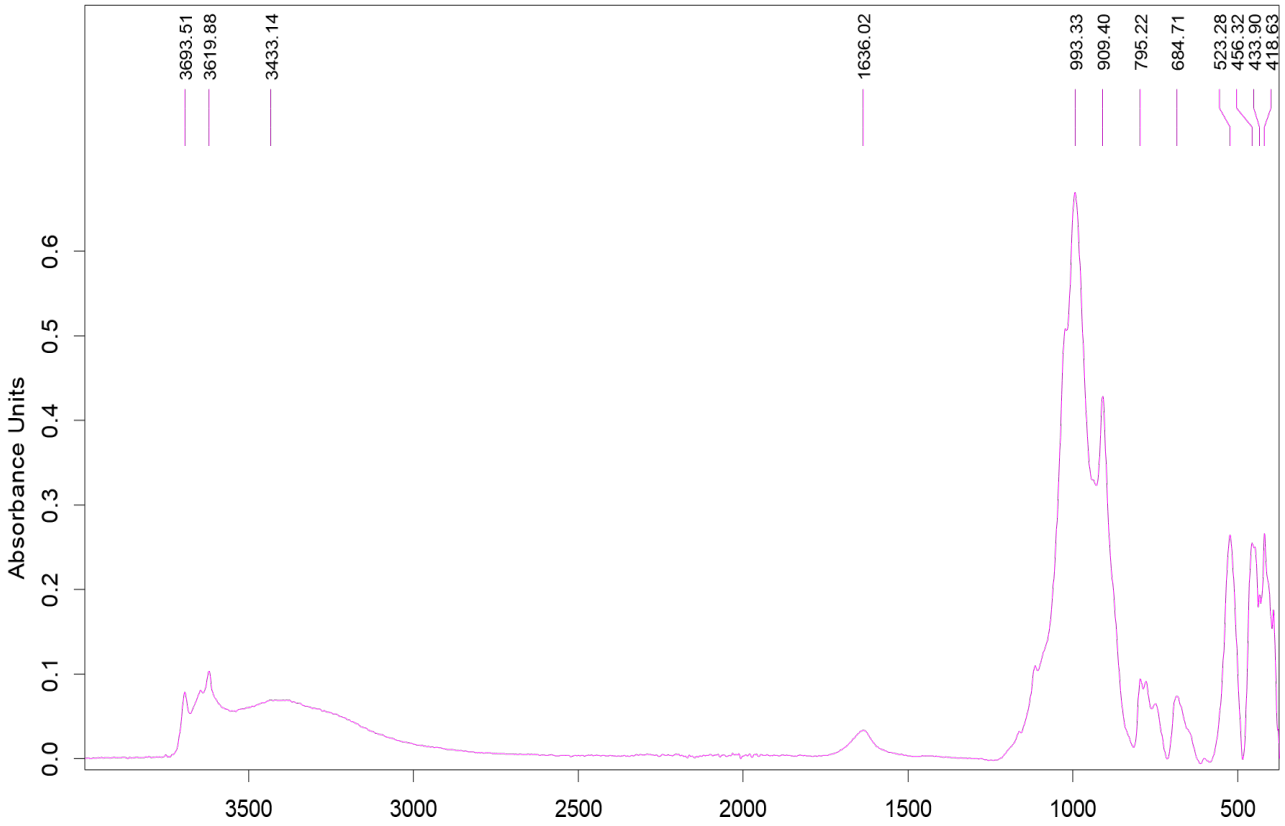
3693.51
3619.88
3433.14
1636.02
993.33
909.40
795.22
684.71
523.28
456.32
433.90
418.63
Absorbance Units
0.0
0.1
0.2
0.3
0.4
0.5
0.6
3500
3000
2500
2000
1500
1000
500

(a)

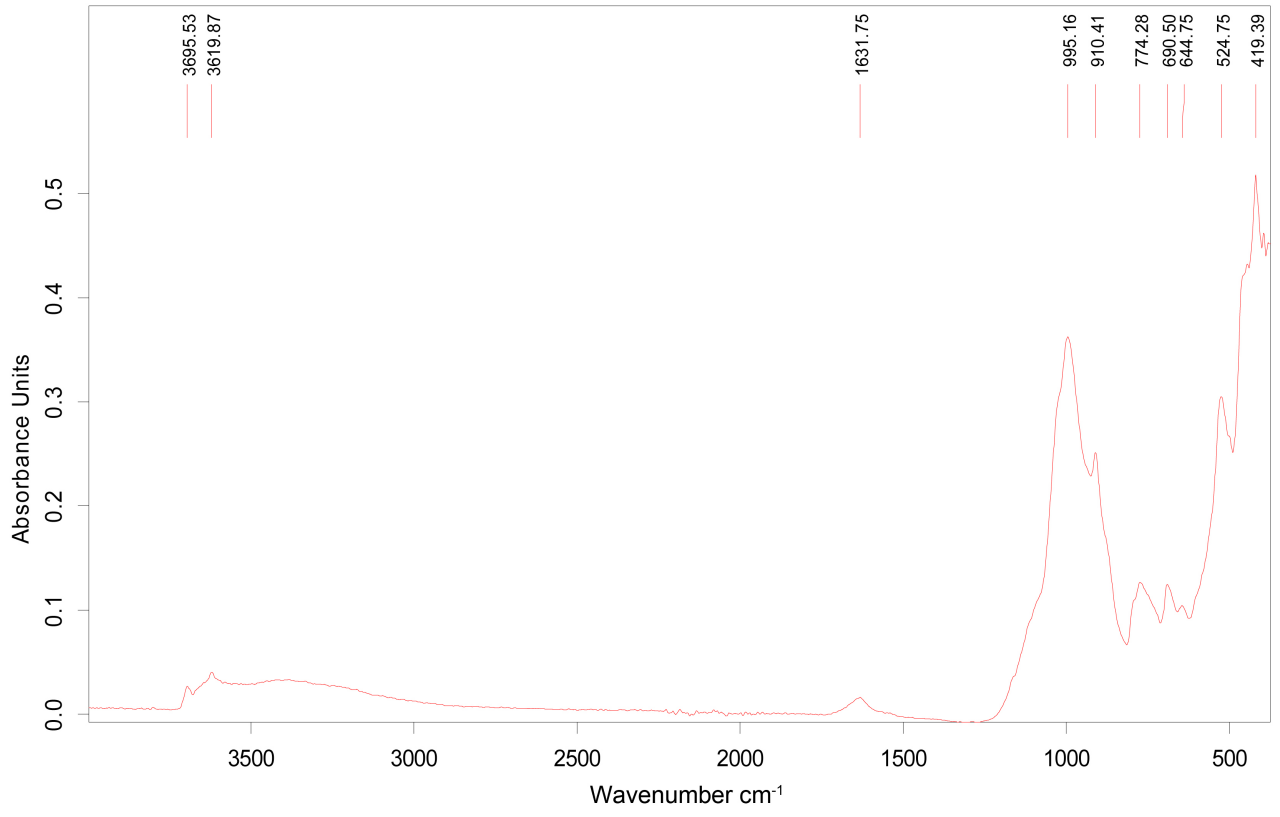
3695.53
3619.87
1631.75
995.16
910.41
774.28
690.50
644.75
524.75
419.39
Absorbance Units
0.0
0.1
0.2
0.3
0.4
0.5
3500
3000
2500
2000
1500
1000
500
Wavenumber cm-1

(b)

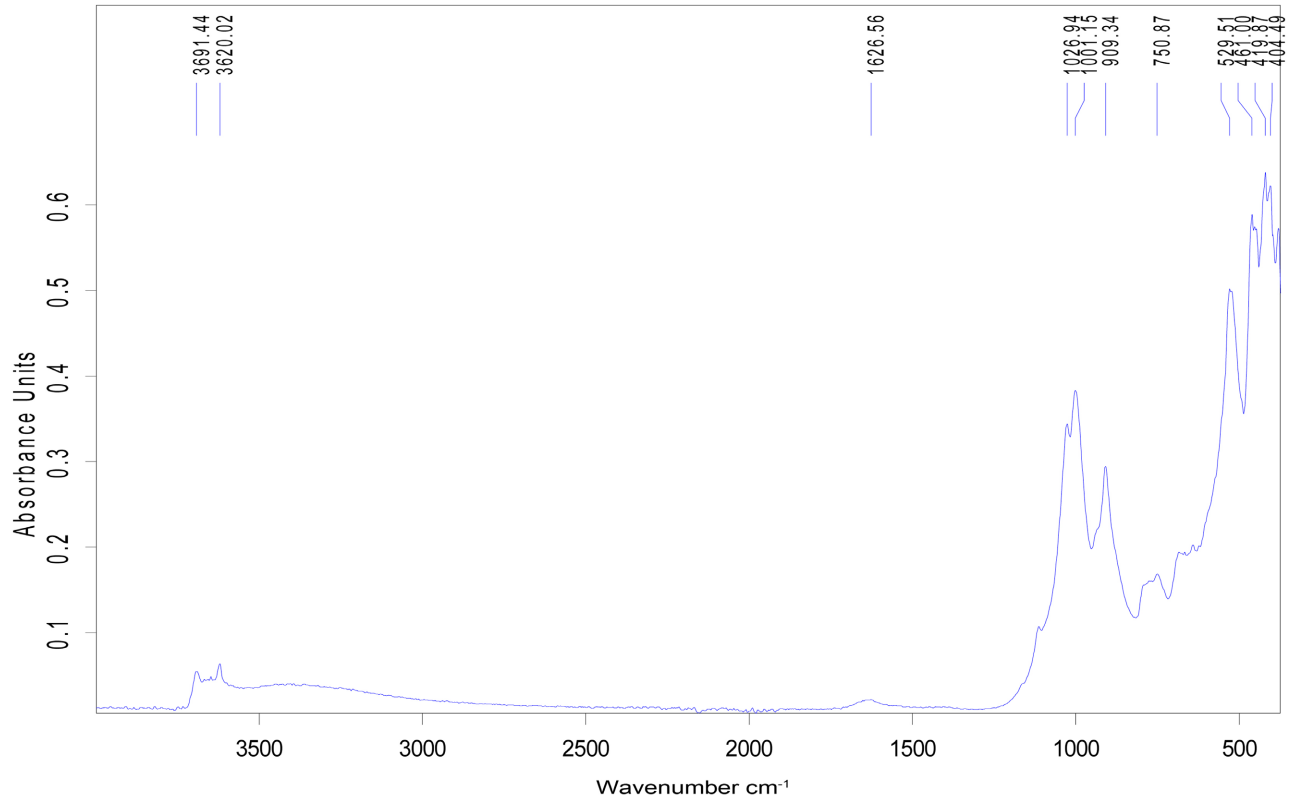


(c)

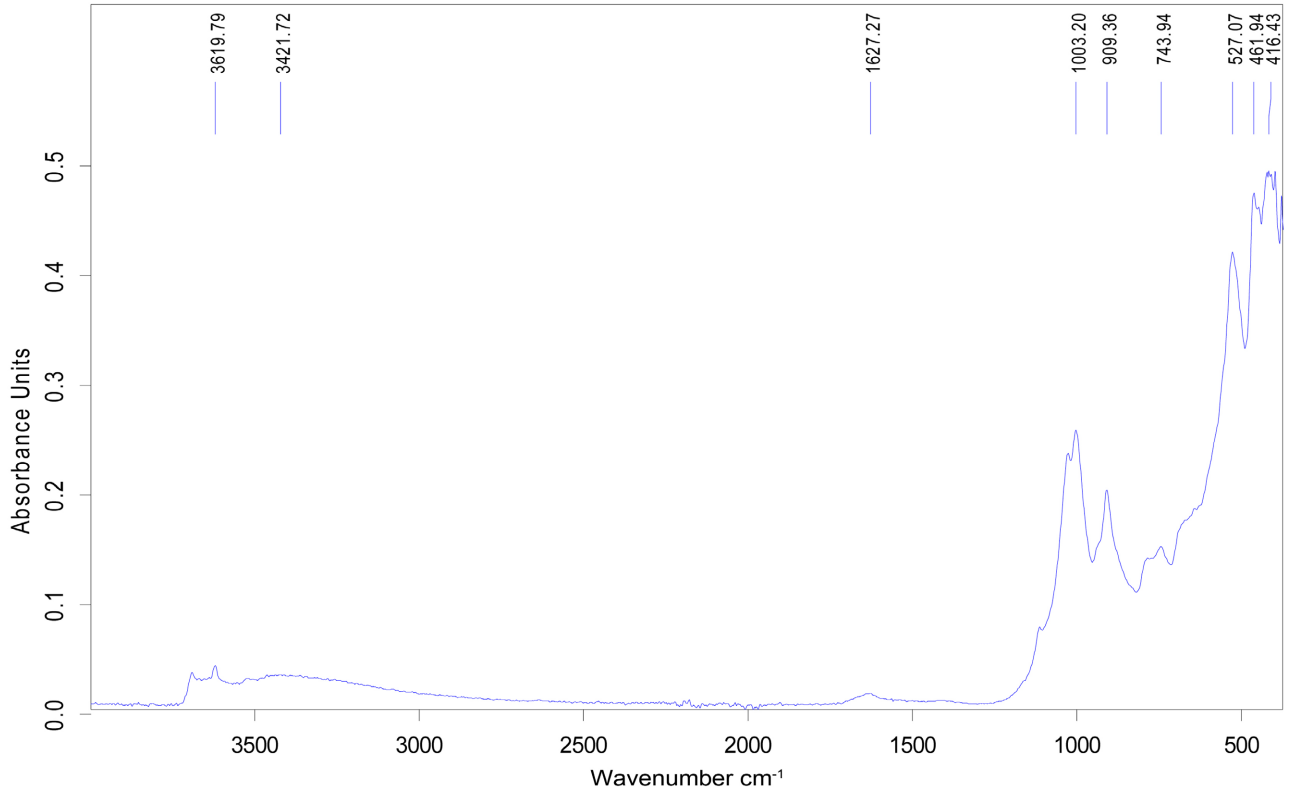


(d)

**Figure 2.** FT-IR spectra of Kao (a), Na-MMT (b), F13 (c) and F23 (d).

774.28 $cm^{-1}$ respectively [20].

**Figure 2(c)** and **Figure 2(d)** show the characteristic peaks around 1300 $cm^{-1}$ centered at 1214 and 1219 $cm^{-1}$; the one at around 730 $cm^{-1}$ centered at 750.87 $cm^{-1}$ and 743.94 $cm^{-1}$ and the wide and strong bond at around 500 $cm^{-1}$ centered at 529.51 $cm^{-1}$ and 527.07 $cm^{-1}$ respectively for F13 and F23 related to bending vibration Ca-O bonds. **Figure 2(d)** shows that the absorption bands at 3691 $cm^{-1}$ and 3620.02 $cm^{-1}$, can be attributed to the interlayer hydroxyl (O-H) and the O-H bonds present in the layer of tetrahedral sheets respectively. The most intensive bands 1026.94 and 1001.15 $cm^{-1}$ for F13 and 1003.20 $cm^{-1}$ for F23 spectra were assigned to the stretching Si-O vibrations of the layer of tetrahedral sheets and those at 461.94 $cm^{-1}$ for F13 and 461 $cm^{-1}$ for F23 are assigned to the bending Si-O-Si vibrations. The characteristic bands at 909.40; 910.41; 909.38 and 909.34 $cm^{-1}$ for Kao, Na-MMT, F13 and F23 respectively are related to Al-O-H vibration. The formation of the formulated clay lime mixtures was confirmed by the disappearance of the absorption bands at 684.71 and 690.50 $cm^{-1}$ for Kao and Na-MMT respectively and the appearance of those at 1214 and 1219 $cm^{-1}$ on the F13 and F23 FT-IR spectra respectively.

It can be observed, from the above results, an excellent correlation between FT-IR analysis and XRD analysis (see **Figure 4** and **Figure 5** Section 3.1.3) of natural clay samples which are the raw materials of those modified clay materials. The quartz was detected in all the samples.

### 3.1.2. SEM Studies of the Clays Materials

The SEM micrographs of Kao (a), Na-MMT (b), F13 (c) and F23 (d) are shown in **Figure 3**. In the SEM micrographs 3a and b, the bright spots show the rough and porous surface of the raw materials, which is one of the factors increasing the preparation yield of F13 and F23 adsorbents. The SEM images 3c and d show the irregular structure of the clay materials and disorder in the pores distributions which can facilitate the intraparticle diffusion of the acid dye. The SEM images 3c and d also show that during the heat treatment, the calcium hydroxide contained in the clay mixtures was dehydrated and converted to calcium oxide, thus leading to the formation of porous calcium-based materials which are responsible for the dye removal. Similar result was reported by [21].

### 3.1.3. XRD Analysis of the Clay Materials

XRD analysis of kaolin shows that kaolinite is the principal constituent. **Figure 4** shows that the main reflections of Ourlago-kaolin (Kao) have appeared at $2\theta$ = 12.36˚, 19.94˚, 24.90˚, 35.98˚, 38.46˚, 45.66˚, 55.12˚ and 62.34˚ [22]. However, this material possesses some impurities. In this clay material, the characteristic peak of maghemite ($Fe_3O_4$ (F)) appears at $2\theta$ = 35.71˚ ($d$ = 2.51Å) [23]. Some crystalline phases can also be observed at the characteristic peaks [24] at $2\theta$ = 20.89˚ ($d$ = 4.23 Å) and 73.67˚ (1.28) for quartz (Q); $2\theta$ = 34.65˚ ($d$ = 2.58 Å) and 62.24˚ (1.49 Å) for montmorillonite and $2\theta$ = 34.65˚ ($d$ = 2.58 Å) for illite (I). **Figure 4** gives XRD pattern of Kao.

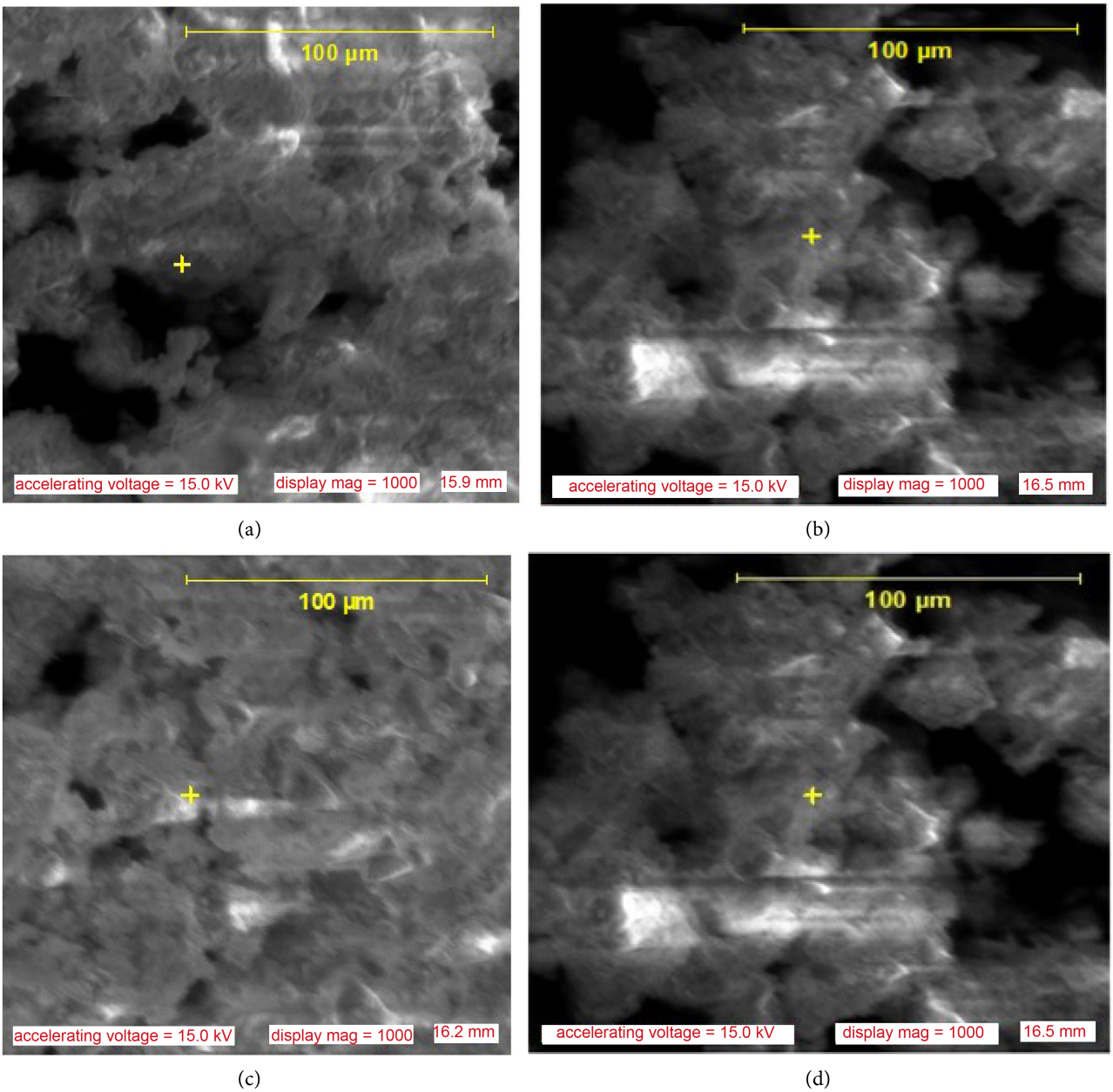


**Figure 3.** SEM Micrographs of: Kao (a); Na-MMT (b); F13 (c) and F23 (d).

**Figure 5** represents the XRD pattern of sodium montmorillonite used in this study as raw material to obtain modified materials. The XRD analysis of this clay shows that montmorillonite is the principal constituent. The main reflections of sodium montmorillonite were observed at $2\theta$ = 6, 24, 23.62, 25.91, 27.88, 34.65, 41.37, 62.07˚ respectively at the characteristic corresponding interlayered spacing $d$(Å): 15.037, 4.50, 3.76, 3.44, 3.19, 2.58, 2.16, 1.49. Other crystalline phases such as quartz; dolomite; illite; calcite; and muscovite in this clay are considered as impurities. They can be observed at the characteristic peaks: $2\theta$ = 20.89, 36.55, 40.34, 45.85, 68.34, 73.67˚ at $d$(Å) = 4.23, 2.45, 2.23, 1.97, 1.45, 1.37, 1.28 respectively for the quartz ($SiO_2$); 2θ = 22.10, 30.92, 59.97˚ at $d$(Å) = 4.02, 2.89, 1.54 for

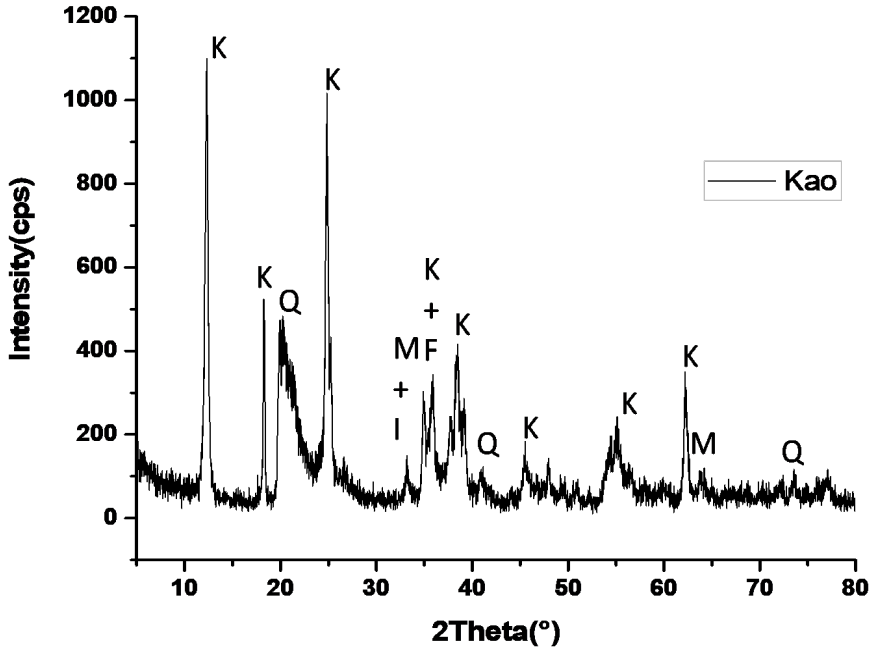


Figure 4. XRD pattern of Kao.

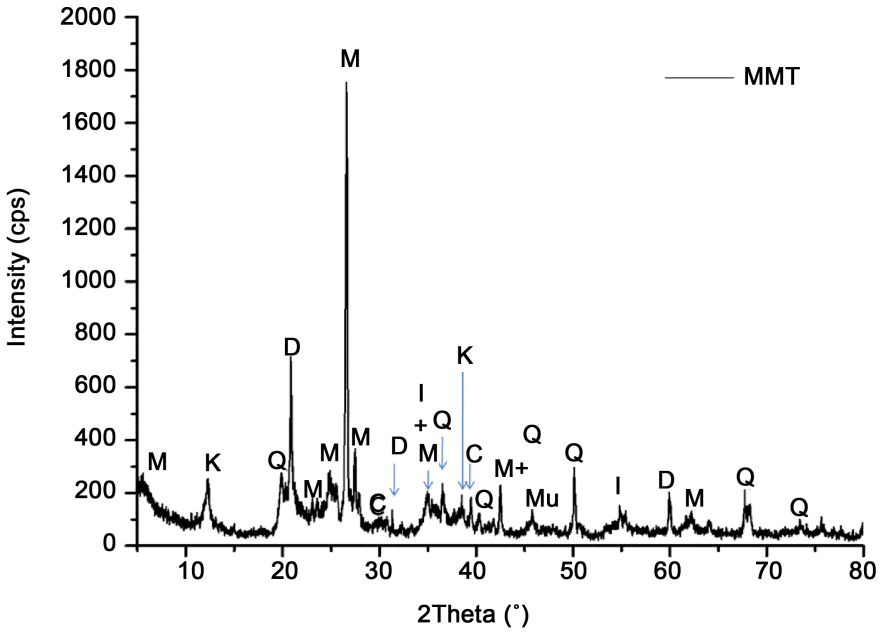


Figure 5. XRD pattern of NaMMT.

dolomite; $2\theta = 29.99, 39.58^{\circ}$ at $d$(Å) = 2.99, 2.27 for calcite (C) and $2\theta = 34.65^{\circ}$, $54.08^{\circ}$ at $d$(Å) = 2.58, 1.69 for illite (I) [24]. Kaolinite (K) and muscovite (Mu) also appeared at $2\theta = 12.21^{\circ}$ ($d = 7.25$ Å) and $38.53^{\circ}$ (2.33 Å) and $2\theta = 45.61^{\circ}$ ($d = 1.99$ Å) respectively according to our database.

Figure 6 represents the XRD patterns of combinations F13 and F23. From these, compared to those of the two raw materials, new crystalline phases emerge. The main reflections of glauconite were observed at $2\theta = 50.07$ and $55.29^{\circ}$

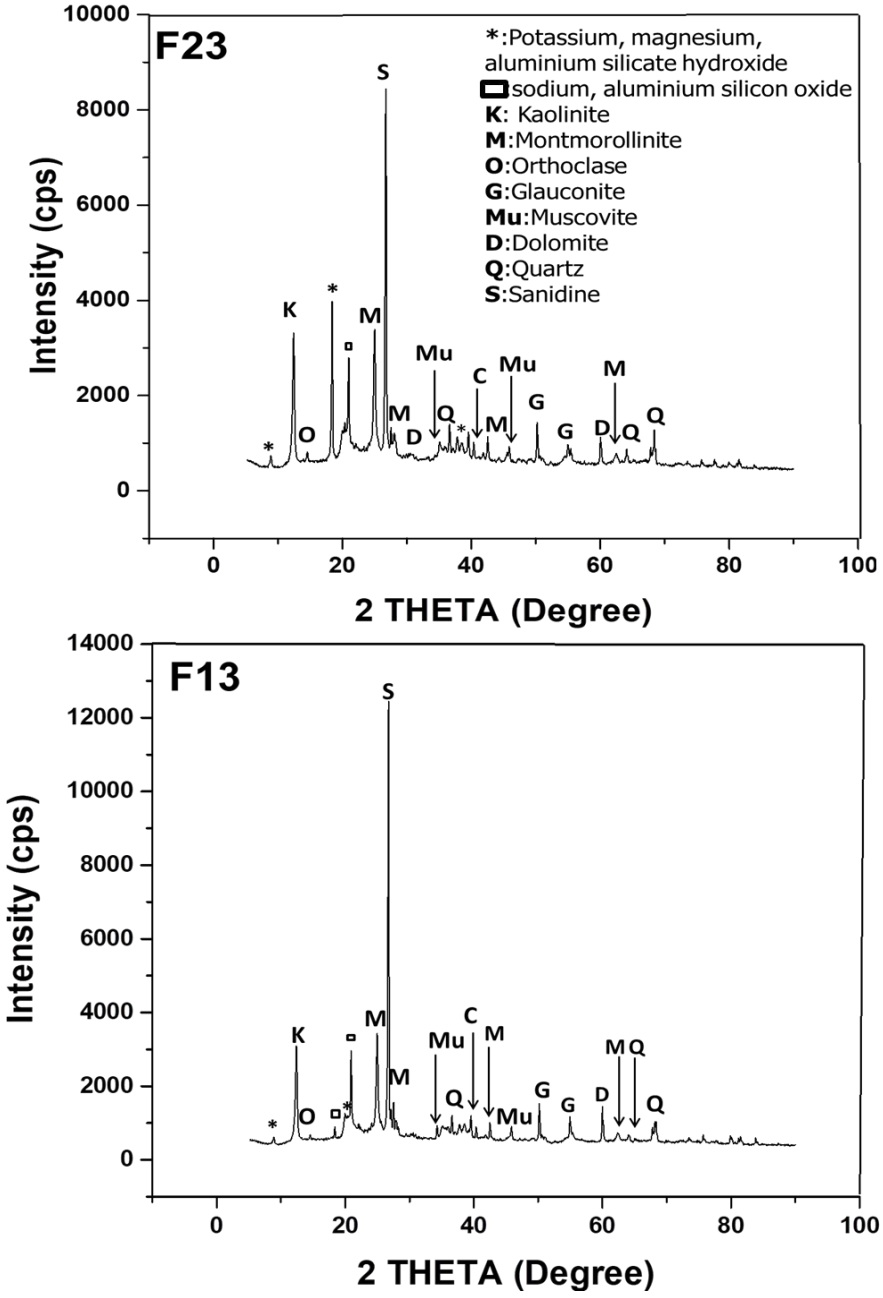


Figure 6. XRD patterns of combinations F13 and F23.

respectively at the characteristic corresponding inter-reticular distances *d*(Å): 1.82 and 1.66; potassium, magnesium, aluminium silicate hydroxide appeared at: 8.88, 19.85 and 37.69˚ respectively at *d*(Å): 9.94, 4.46 and 2.38., Sanidine also appeared at 26.75˚ (3.33 Å) [24]; Orthoclase appeared at: 13.32˚ ($d = 6.63$ Å) [25]; sodium aluminium silicon oxide appeared at: 19.71˚ and 20.04˚ respectively at *d*(Å): 4.50 and 4.42 [26]. From the above, with regard to diffractograms of F13 and F23, an additional peak of glauconite was detected at 55.29˚ (1.66 Å) in F13 and the high intensities of the various characteristic peaks of different crystalline phases observed testify to the quality of the treat-

ment carried out.

### 3.1.4. TG-DSC Analysis of the Clay Materials

Figure 7 represents the TG-DSC graphs of Kao (a), Na-MMT (b), F13 (c), F23 (d). Figure 7(a) shows that between 20˚C - 200˚C, there is an endothermic peak at 59˚C in DSC graph, here, the mass loss of Kao can be assigned to the departure of water present on the clay material surface. Figure 7(b) shows that in the temperature range of 20˚C - 200˚C, there is an endothermic peak at 53˚C in DSC graph, the mass loss of Na-MMTin this step can be due to the departure of the physically adsorbed water at the clay surfaces and water molecules around sodium ion on the sites where the exchange is possible in MMT [20]. Figure 7(b) also shows that a thermal bump between 300˚C and 330˚C is concomitant with a significant weight loss.

Figure 7(c) and Figure 7(d) show that between 20˚C - 200˚C, the endothermic peaks precisely at 65˚C for F13 and F23 are associated to the liberation of the O-H of the physisorbed $H_2O$ followed by the mass losses of 4.90% for F13 and 4.54% for F23. Figure 7(a), Figure 7(c) and Figure 7(d) show that above 450˚C, very marked endothermic phenomena centered at 483˚C, 503˚C and 502˚C respectively, are associated with significant weight loss. This leads to the dehydroxylation of kaolinite [23] according to the equation:

$$\underset{\text{(Kaolinite)}}{Si_2Al_2O_5(OH)_4} \rightarrow \underset{\text{(Metakaolin)}}{Si_2Al_2O_7} + 2H_2O$$

Table 4 indicates that the total weight loss of F13 and F23 is higher than those of the Ourlago kaolin (Kao) and the sodium montmorillonite (Na-MMT). This can be due to the transformation of calcium hydroxide into calcium oxide during the calcination step. This increase of the total weight loss confirms that the modification was accomplished.

### 3.1.5. EDX Analysis of the Clay Materials

Figure 8(a), Figure 8(c) and Figure 8(d) show that the main elements of Kao, F13 and F23 are silicium (Si), oxygen (O), iron (Fe), potassium (K) and aluminium (Al). Figure 8(b) shows that the main elements of Na-MMT are silicium (Si), oxygen (O), sodium (Na), iron (Fe), and aluminium (Al). The silicium (Si) presence in these samples also induced the presence of the quartz which is confirmed by XRD and FT-IR analyses in the previous section.

Table 5 shows that the ratio of Al/Si is around 1.5 times greater of Na-MMT than those of Kao, F13 and F23 due to the purification step of the natural montmorillonite clay. This elemental composition also shows that these materials are aluminosilicates.

### 3.1.6. BET Surface Area of the Clay Materials

In many applications, porosity of clay materials is one of the desired parameters. The BET surface area and pore volume of adsorbents were measured and results are reported in Table 6. This table compares the porosity of both raw and modified clay materials. Modified clay materials F13 and F23 give ~ 4.4 to 9.6 times

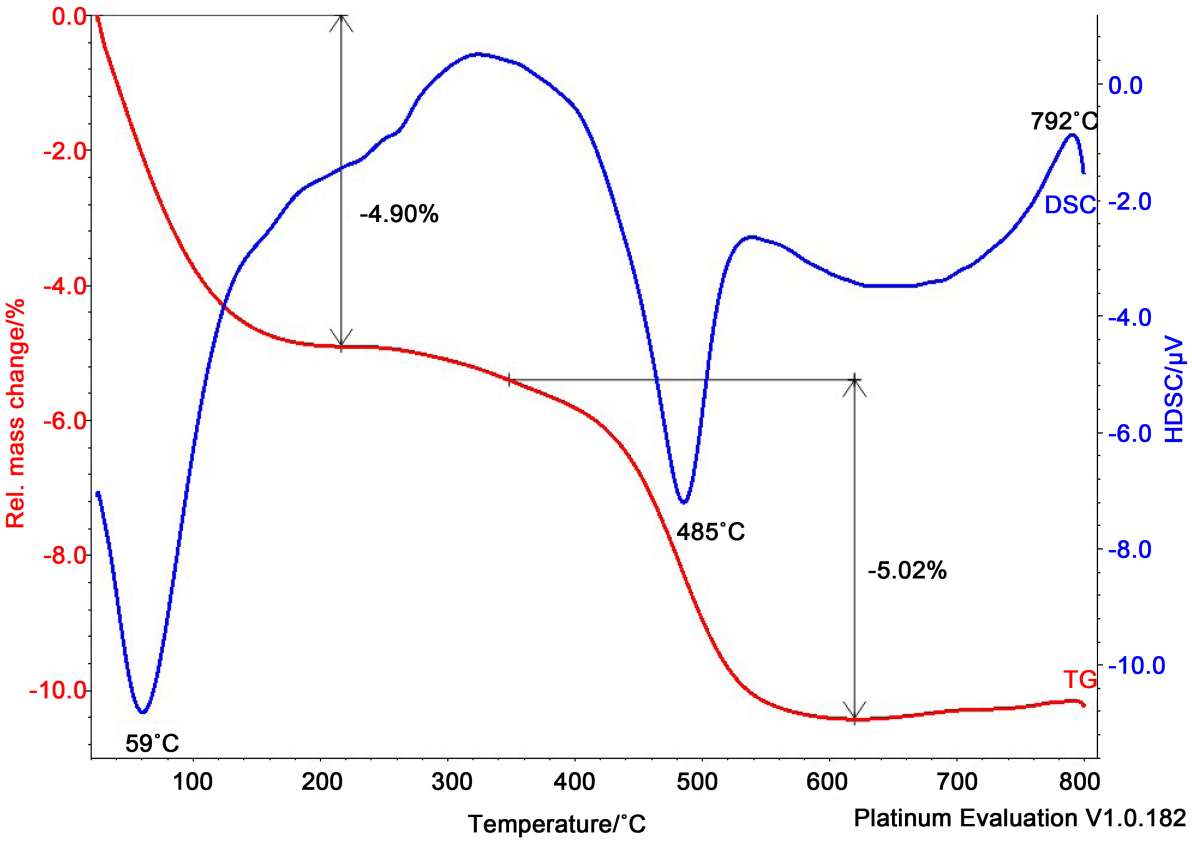
0.0
-2.0
-4.0
-6.0
-8.0
-10.0
Rel. mass change/%
-4.90%
792°C
DSC
485°C
-5.02%
TG
59°C
100
200
300
400
500
600
700
800
Temperature/°C
0.0
-2.0
-4.0
-6.0
-8.0
-10.0
HDSC/μV
Platinum Evaluation V1.0.182

(a)

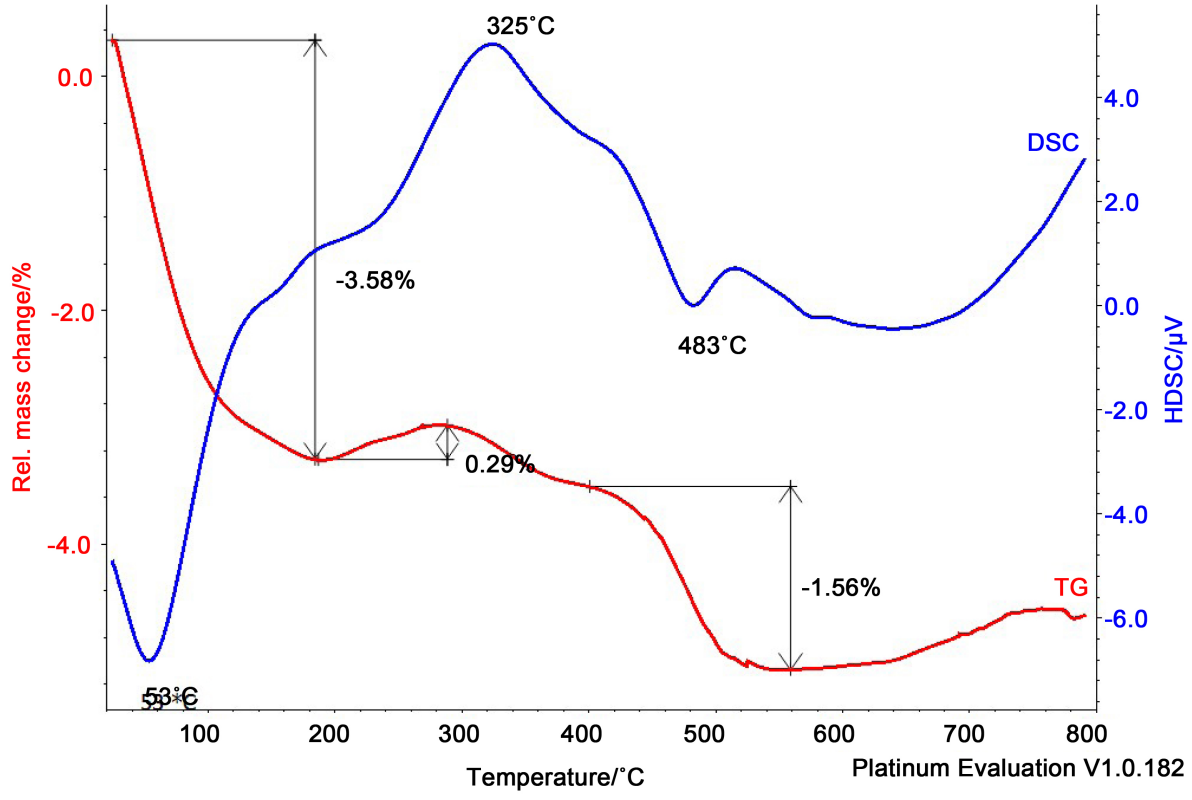
325°C
0.0
-2.0
-4.0
Rel. mass change/%
-3.58%
DSC
483°C
0.29%
-1.56%
TG
53°C
100
200
300
400
500
600
700
800
Temperature/°C
4.0
2.0
0.0
-2.0
-4.0
-6.0
HDSC/μV
Platinum Evaluation V1.0.182

(b)

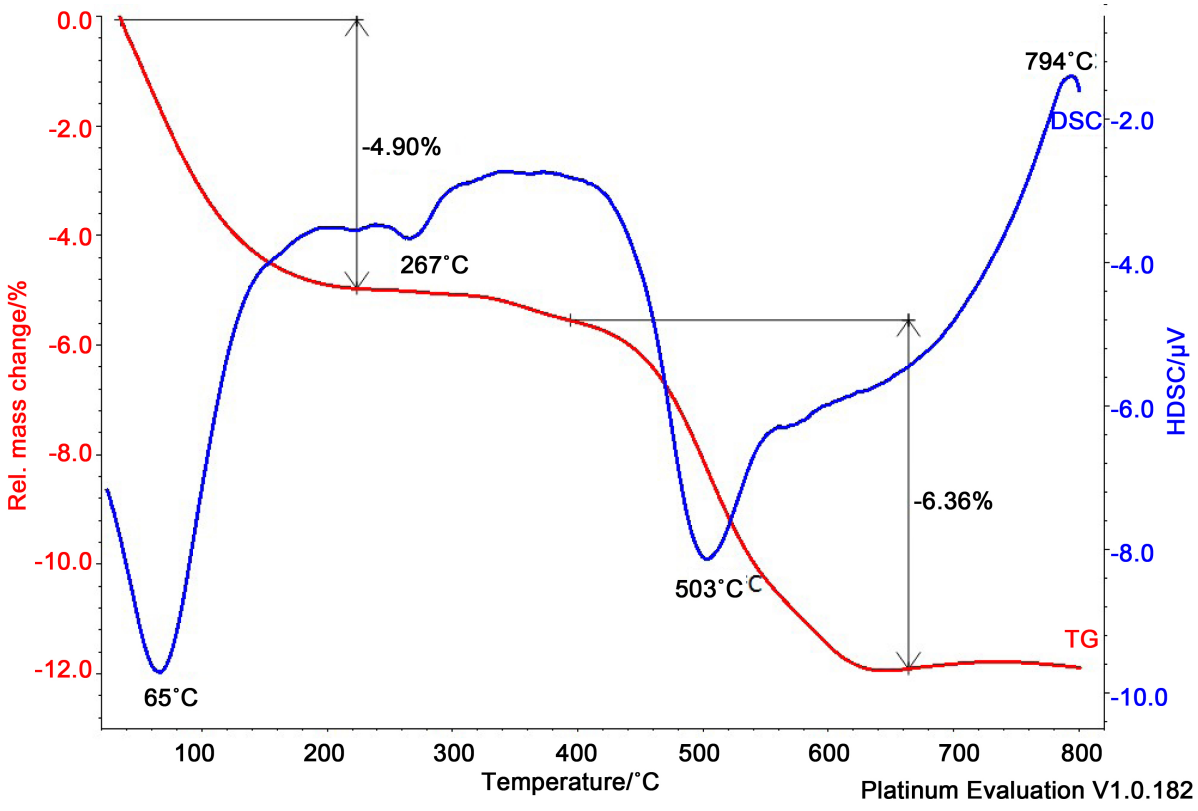


(c)

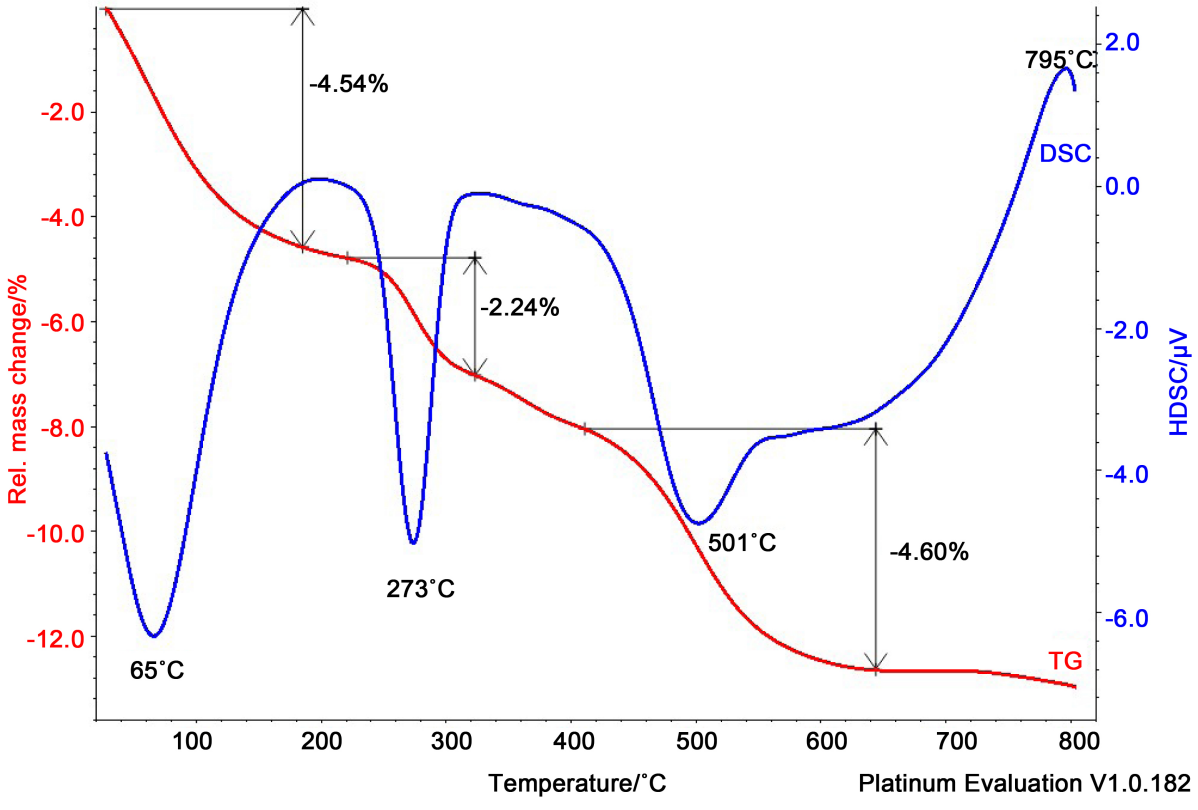


(d)

**Figure 7.** TG-DSC curves of: Kao (a); Na-MMT (b); F13 (c) and F23 (d).

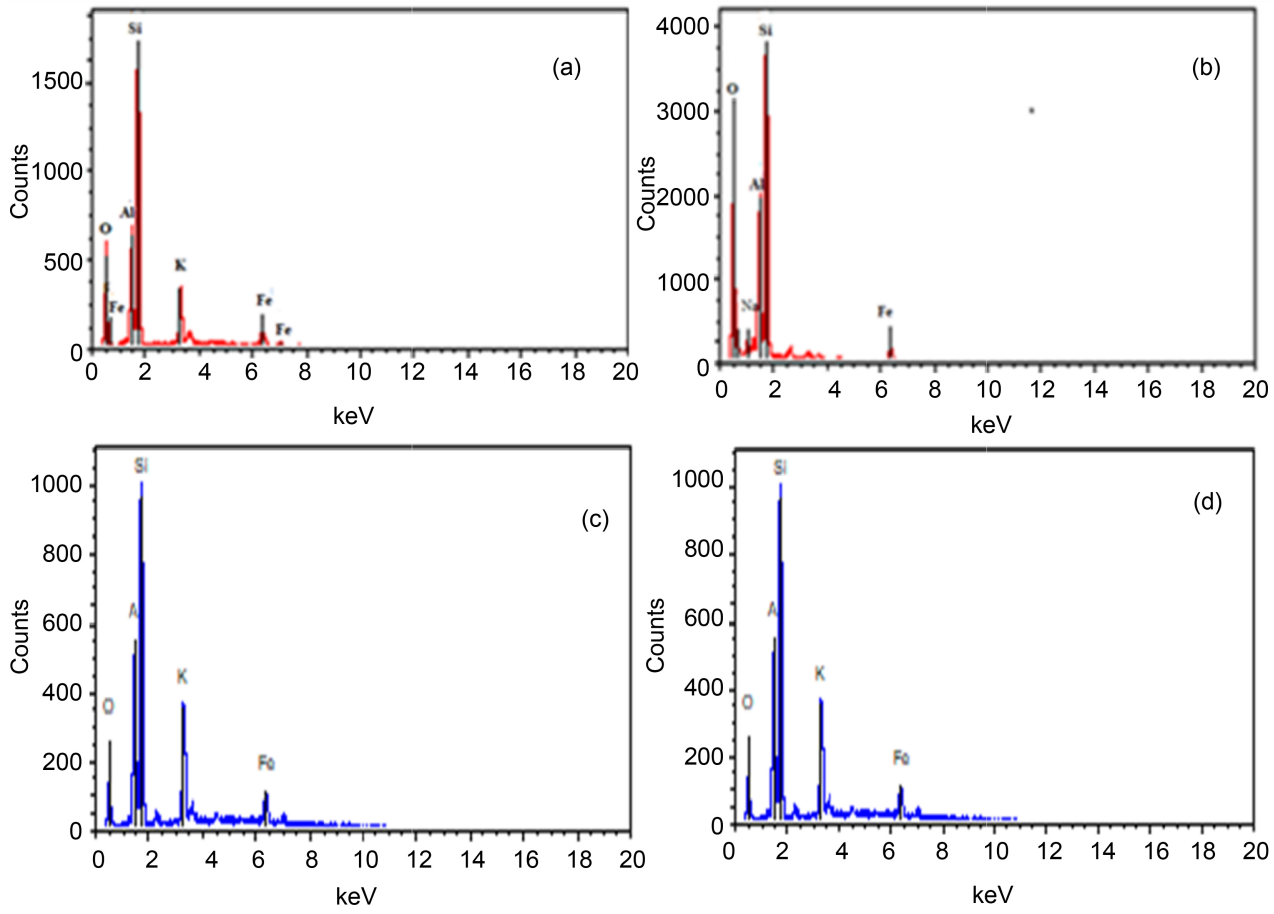


**Figure 8.** EDX spectra of: Kao (a); Na-MMT (b); F13 (c) and F23 (d).

**Table 4.** The weight loss of clay materials at different steps.

| Temperature range | Weight loss (%) of clay materials | | | |
|---|---|---|---|---|
| | Kao | Na-MMT | F13 | F23 |
| 20˚C - 200˚C | 4.90 | 3.58 | 4.90 | 4.54 |
| 200˚C - 600˚C | 5.02 | 1.85 | 6.36 | 6.84 |
| 600˚C - 800˚C | / | / | / | / |
| Total | 9.92 | 5.43 | 11.26 | 11.38 |

**Table 5.** Percentage of some constituents of Kao, Na-MMT, F13 and F23.

| Element (%) | Kao | Na-MMT | F13 | F23 |
|---|---|---|---|---|
| Al | 4.2 | 5.5 | 6.1 | 5.9 |
| Si | 30.5 | 34.1 | 30.2 | 29.8 |

increases in surface area. A substantial decrease in BJH adsorption average pore radius can also be observed and a rise in pore volume suggests the formation of new pore through the synthesis procedure. Similar results were reported by Rehman *et al.* [27].

**Table 6.** Porosity characteristics of clay materials.

| Property | Clay materials | | | |
|---|---|---|---|---|
| | Kao | Na-MMT | F13 | F23 |
| BET Surface Area ($m^2 \cdot g^{-1}$) | 13.8351 | 30.4331 | 133.0071 | 132.3481 |
| Pore Volume ($cm^3 \cdot g^{-1}$) | 0.069501 | 0.088159 | 0.262011 | 0.249102 |
| BJH Adsorption average pore radius (2V/A) (Å) | 112.536 | 67.831 | 51.316 | 54.193 |

## 3.2. Adsorption Mechanism

### 3.2.1. Agitation Time Effect on the Amounts of AO52 Dye Adsorbed Onto Kao, Na-MMT, F13 and F23

**Figure 9** shows the agitation time intervals ranging from 0 to 40 min. The uptake of AO52 dye (mg/g) onto Kao, Na-MMT, F13 and F23 increased rapidly within the first 3 min for each adsorbent and then increased slowly until reached the equilibrium and remained nearly constant. The equilibrium times are 5 min for Kao and F23; 10 min for Na-MMT and F13. The very high adsorption capacities observed during this first step can lead to the disponibility and accessibility of many active sites which also increased after the modification step of the natural clays. A rise in agitation time and the adsorption rate could induce a reduction of the boundary layer resistance, the transport of the AO52 dye from the solution to the sorbent surfaces, the migration of the AO52 dye at the interface of adsorbent - solution as well as its intraparticle diffusion in the adsorbents internal pores and into the cavities present on the surface during an adsorption process. Similar results were reported by Abbas *et al.* [28].

### 3.2.2. pH Effect on the Amounts of AO52 Dye Adsorbed by Kao, Na-MMT, F13 and F23

**Figure 10** shows that with the natural clays, when the pH increases from 2 to 12, the quantity of AO52 dye removed at equilibrium ($q_e$) varied from 0.6789 to 0.1396 mg/g for Na-MMT and 0.4995 to 0.0282 mg/g for Kao. As the pH of the solution increases, the electrostatic force repulsions are higher between the adsorbent and the acid dye, thereby decreasing the extent of adsorption. The higher adsorption of AO52 dye onto natural clays could also be attributed to hydrophilic interaction, the positive charge of the edge sites of the clay materials surface enhances the electrostatic interaction and the lone pair electrons on the nitrogen may be attracted to the positively charged samples surfaces at the low pH [29]. Conversely, the amount of AO52 adsorbed onto calcined mixed clays and lime F13 and F23 increase when the pH increases, according to this equation:

$$\mathrm{SiO_2(s)} + x\mathrm{Ca^{2+}(aq)} + 2x\mathrm{OH^-(aq)} + (y-x)\mathrm{H_2O} \rightarrow x\mathrm{CaO \cdot SiO_2} \cdot y\mathrm{H_2O}$$

where $x$ is 0.8 - 1.5 and $y$ is 0.5 - 2.5, when the hydroxide ion ($OH^-$) concentration is higher, the $SiO_2$ contained in the structure of clay dissolves and combines with calcium ions to give porous structure and large specific surface materialsnamely calcium silicates [21]. The resulting porous materials in this

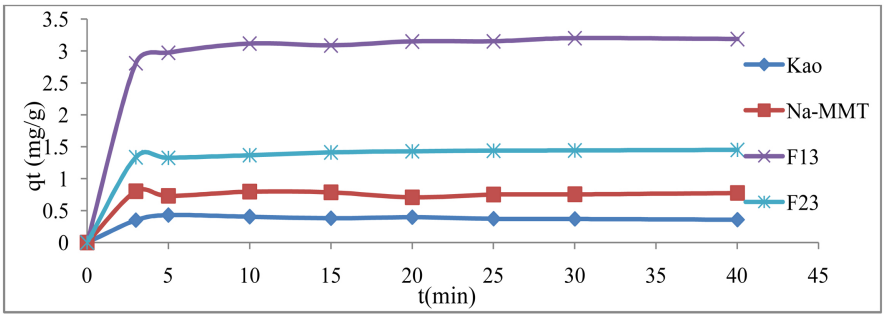


**Figure 9.** Agitation time effect on the AO52 dye removal onto Kao, Na-MMT, F13 and F23 (pH = 2, $R$ = 5 g/L, $C_o$ = 10 mg/L, $T$ = 25˚C, stirring speed = 250 rpm, sorbent size = 80 μm).

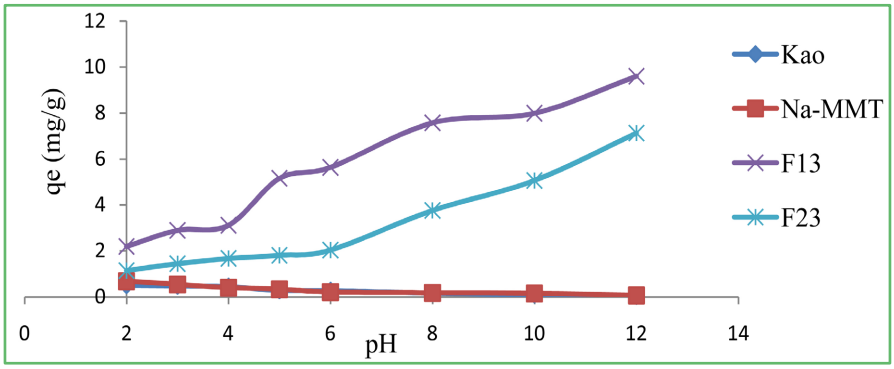


**Figure 10.** pH effect on the removal of AO52 dye onto different adsorbent ($R$ = 5 g/L; stirring speed = 250 rpm; $C_o$ = 10 mg/L; $T$ = 25˚C, size of sorbent = 80 μm).

medium enhance the removal of the AO52 dye molecules. So at high pH, the solution in contact with the basal oxygen surface of the tetrahedral sheet will contain excess hydroxyls and thus the surface exhibited a CEC [30].

### 3.2.3. Adsorbent Dosage Effect on the Removal of AO52 Dye Molecules

The influence of the Kao, Na-MMT, F13 and F23 dosage is shown in **Figure 11**. This figure shows that when the mass of adsorbent varied from 0.1 - 0.8 g/20mL, the variation of 0.578 to 0.2288 mg/g for Kao; 0.8899 to 0.5157 mg/g for Na-MMT; 5.1579 to 1.4122 mg/g (64.47% to 88.26%) for F13 and 2.0589 to 0.6635 mg/g (51.47% to 82.94%) for F23 was observed after each sample equilibrium time. These results show that the AO52 dye removal capacities increase when the adsorbent dosage decreases. At this adsorbent dosage, there is a variation of the AO52 dye solution pH. Here; it can be also observed that the exchange of anion with acid dye and the adsorbent active surface functional groups is the possible reaction. Similar results were reported by Saad *et al.* [31]. A higher percentage of removal of pollutants may be observed by increasing the dosage of the clay materials. This is probably because of the availability of a greater number of active sites for AO52. However, no significant increase in the percentage removal of AO52 was observed as the dosage of adsorbent increased, probably because of the attainment of equilibrium. Similar results were reported by Zahir *et al.* [32].

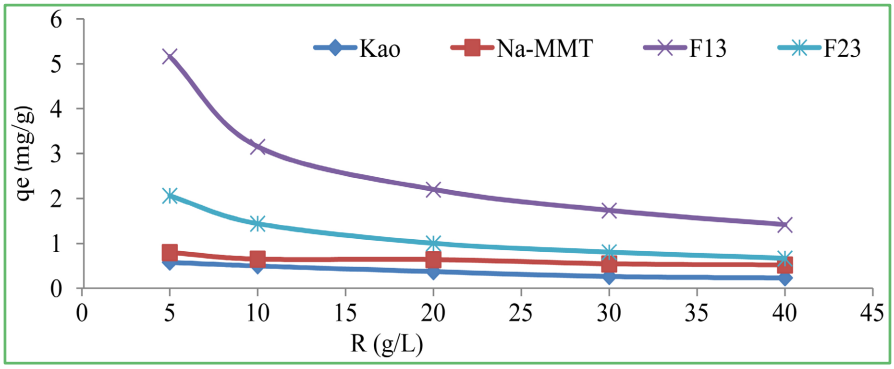


**Figure 11.** Adsorbent dosage effect on AO52 dye adsorption onto adsorbents ($C_o$ = 10 mg·L$^{-1}$, pH = 2, $T$ = 25˚C, stirring speed = 250 rpm, sorbent size = 80 µm).

### 3.2.4. Effect of AO52 Dye Concentration with the Adsorption Capacities by Kao, Na-MMT, F13 and F23

**Figure 12** shows that the initial AO52 dye concentration strongly affects adsorption capacity. Increasing of AO52 concentration will also increase the AO52 dye diffusion around the clay material surface due to overcoming the various mass transfer resistances at the solution-adsorbent interface, thereby resulting in strong collisions between the dye and the catalytic area as a consequence of an extension in the strength of the propulsion of the facilitated diffusion [33] [34].

### 3.2.5. Temperature Effect on the Removal of AO52 Dye by Kao, Na-MMT, F13 and F23

Temperature is one of the kinetic parameters that increases through the outer layer and internal broods of the adsorbent materials, the diffusion of the adsorbate molecules. **Figure 13** shows that the uptake ability of AO52 dye on Na-MMT increases when the temperature increases with values of 0.792 to 1.9468 mg·g$^{-1}$ at 298 to 333 K, this can be due to the great mobility of the AO52 dye molecules, thus facilitating their penetration and their accessibility at the level of the catalytic area of the porous surface of Na-MMT. This will result in suppression of the energy of activation and furthermore increase the diffusion rate of the intra-particle. Similar results were reported by [35].

**Figure 13** also indicates that the capacities of adsorption at equilibrium of Kao, F13 and F23 decrease from 0.3815 to 0.0715 mg·g$^{-1}$; 3.1158 to 0.5052 mg·g$^{-1}$ and 1.4105 to 0.941 mg·g$^{-1}$ respectively with the temperature increasing from 298 to 333 K and the adsorption phenomenon controlled by exothermic process. The decrease in the adsorption of AO52 dye by clay materials Kao, F13 and F23 with the increase in the temperature of the reaction medium could be due to the improvement in desorption during the adsorption process as well as to the undermining of the physical attraction contraint at the interface of catalytic area and CI Acid Orange 52. Similar result was obtained by [36]. According to the above results, physical adsorption could play an important role in this system. Similar result was reported by Chen *et al.* [20].

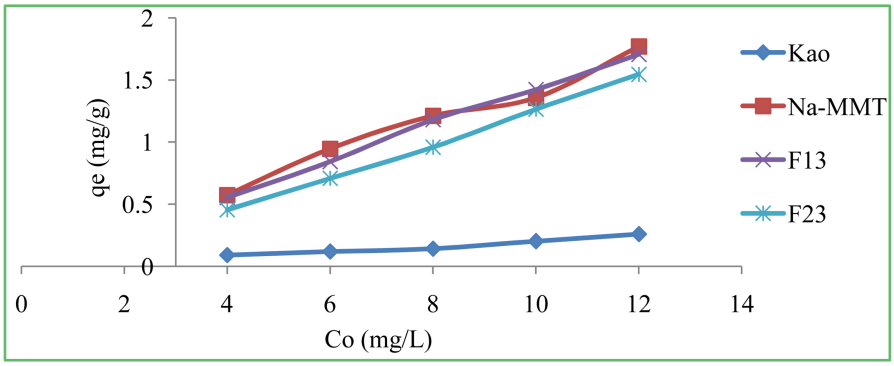


**Figure 12.** Initial AO52 dye concentration effect on the adsorption capacities of Kao, Na-MMT, F13 and F23 (pH = 2, $R$ = 5 g·L$^{-1}$, $T$ = 25˚C, stirring speed = 250 rpm, sorbent size = 80 µm).

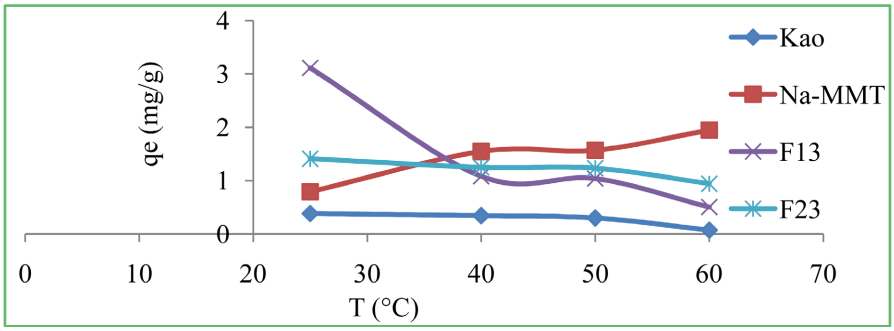


**Figure 13.** Temperature effect on the removal of AO52 dye by Kao, Na-MMT, F13 and F23 at different equilibrium time (pH = 2, $R$ = 5 g/L, $C_o$ = 10 mg·L$^{-1}$, sorbent size = 80 µm).

## 3.3. Isotherm Study

### 3.3.1. Langmuir Sorption Model

Langmuir isothermal plot for the removal of AO52 by Kao, Na-MMT, F13 and F23 is shown in **Figure 14**.

### 3.3.2. Isothermal Model of Freundlich

**Figure 15** shows the plot of the Freundlich isotherm for the removal of AO52 by Kao, Na-MMT, F13 and F23.

**Table 7** represents the Langmuir and Freundlich adsorption isotherms for the removal of AO52 dye using Kao, Na-MMT, F13 and F23.This table shows that the uptake of AO52 dye by the clay mixtures F13 and F23 exceeded the AO52 dye adsorption capacity for single-layer adsorption, is overwhelmed, which could explain why even multilayer adsorption is produced or any other possible mechanism. For example, precipitation would also occur during this process. Values of n greater than one made it possible to conclude that the Freundlich model for F13 and F23 allows a better adaptation of this study [21]. Values of $R^2$ are higher for the Langmuir model, this suggests that the adsorption sites possess the same energy and there is monolayer of AO52 dye molecules adsorbed at the clays surface.

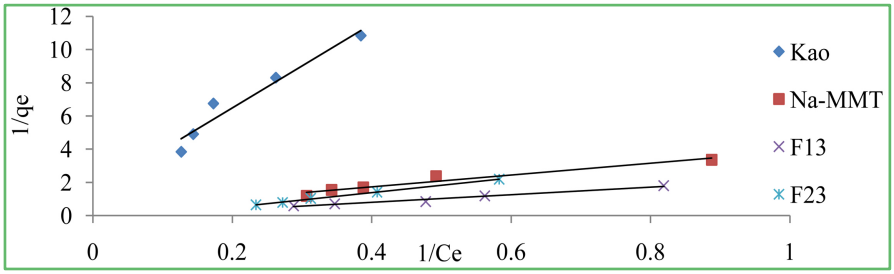


**Figure 14.** Isothermal plot of Langmuir for the removal of AO52 by Kao, Na-MMT, F13 and F23.

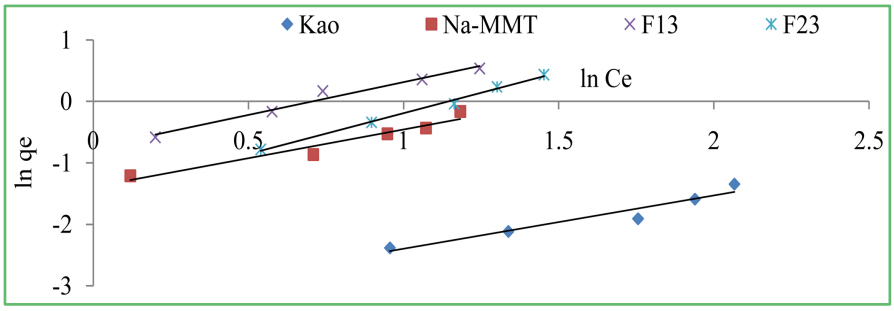


**Figure 15.** Plot of the Freundlich isotherm for the removal of AO52 dye by Kao, Na-MMT, F13 and F23.

**Table 7.** Langmuir and the Freundlich adsorption isotherms for the removal of AO52 dye usingKao, Na-MMT, F13 and F23.

| Clay materials | Langmuir adsorption isotherm | | | Freundlich adsorption isotherm | | |
|---|---|---|---|---|---|---|
| | $q_{max}$ (mg·g$^{-1}$) | $K_L$ (L·mg$^{-1}$) | $R^2$ | $n$ | $K_f$ (g·mg$^{-1}$·min$^{-1}$) | $R^2$ |
| Kao | 0.8761 | 0.0451 | 0.945 | 0.7507 | 0.03815 | 0.931 |
| Na-MMT | 2.6178 | 0.089 | 0.945 | 0.9354 | 0.2483 | 0.938 |
| F13 | 7.874 | 0.055 | 0.977 | 1.5000 | 0.4691 | 0.971 |
| F23 | 3.1645 | 0.0865 | 0.998 | 1.0718 | 0.2174 | 0.993 |

Table 8 shows that, at different concentrations of AO52 dye at 25˚C, the $R_L$ values are amidst 0 - 1, thus confirming therefore that favorable adsorption process. These low $R_L$ values prove that the interactions between the AO52 dye molecules and the clay materials used are strong. A similar result was reported by Kumar and Tamilarasan [36].

## 3.4. Study of Kinetic Models

### 3.4.1. Pseudo First Order Kinetic Model

Figure 16 shows pseudo first order kinetic model for AO52 dye removal onto Kao, Na-MMT, F13 and F23.

### 3.4.2. Pseudo Second Order Kinetic Model

Pseudo second order kinetic models for AO52 dye adsorption onto Kao, Na-MMT, F13 and F23 are shown in Figure 17.

**Table 8.** $R_L$ values for the removal of AO52 dye by the clay materials at 25˚C.

| AO52 dye initial concentration (mg·L$^{-1}$) | | 4 | 6 | 8 | 10 | 12 |
|---|---|---|---|---|---|---|
| $R_L$ | Kao | 0.8471 | 0.7870 | 0.7348 | 0.6891 | 0.6488 |
| | Na-MMT | 0.7374 | 0.6518 | 0.5841 | 0.5291 | 0.4835 |
| | F13 | 0.8196 | 0.7518 | 0.6944 | 0.6451 | 0.6024 |
| | F23 | 0.3936 | 0.3020 | 0.2450 | 0.2280 | 0.1778 |

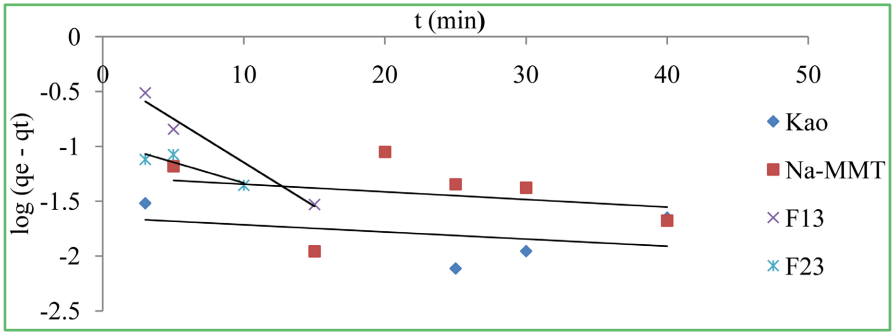


**Figure 16.** Pseudo first order kinetic model for AO52 dye removal by Kao, Na-MMT, F13 and F23 at 298 K.

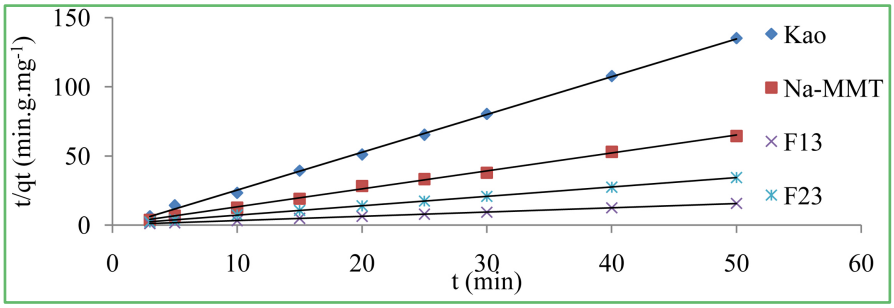


**Figure 17.** Pseudo-second-order kinetic models for AO52 dye removal onto Kao, Na-MMT, F13 and F23 at 298 K.

Table 9 represents the various constants resulting from these two kinetic models used in this study. In view of the results presented in Table 6, the pseudo second order kinetic model makes it possible to describe with more precision the mechanism of adsorption of the AO52 dye molecules. This is due to the fact that the real values ($q_{e,exp}$) are close to the theoretical ($q_{e,cal}$) values. In addition, from this model, it emerges that the values of the correlation coefficients ($R^2$) are very high and almost equal to one for all the adsorbents.

## 3.5. Thermodynamic Study

Figure 18 represents the plot of $\ln K_d$ vs $1/T$ for clay materials at temperatures 298, 313, 323 and 333 K.

The different thermochemical data $\Delta G^\circ$, $\Delta H^\circ$ and $\Delta S^\circ$ for the retention of AO52 dye by Kao, Na-MMT, F13 and F23 are shown in Table 10.

**Table 9.** Various constants result from these two kinetic models.

| Pseudo-first-order model | | | | |
|---|---|---|---|---|
| Samples | $k_{1,ads}$ (min$^{-1}$) | Real $q_{e,exp}$ (mg·g$^{-1}$) | Calculated $q_{e,cal}$ (mg·g$^{-1}$) | $R^2$ |
| Kao | 0.013818 | 0.3805 | 0.02238 | 0.138 |
| Na-MMT | 0.013818 | 0.796 | 0.05296 | 0.062 |
| F13 | 0.181937 | 3.1158 | 0.4446 | 0.971 |
| F23 | 0.085211 | 1.4105 | 0.11066 | 0.823 |
| Pseudo-second-order model | | | | |
| Samples | $k_{2,ads}$ (g·mg$^{-1}$·min$^{-1}$) | Real $q_{e,exp}$ (mg·g$^{-1}$) | Theoretical $q_{e,cal}$ (mg·g$^{-1}$) | $R^2$ |
| Kao | / | 0.3805 | 0.36589 | 0.999 |
| Na-MMT | 7.84837 | 0.796 | 0.76982 | 0.997 |
| F13 | 0.71716 | 3.1158 | 3.22581 | 0.999 |
| F23 | 1.29542 | 1.4105 | 1.46842 | 0.999 |

**Table 10.** Thermodynamic constants of the removal of CI Acid Orange 52 on the clay materials (sorbent mass = 0.5 g; $V$ = 100 mL; $C_o$ = 10 mg·L$^{-1}$; pH = 2).

| Clay materials | Temperature (K) | $\Delta H^\circ$ (kJ·mol$^{-1}$) | $\Delta S^\circ$ (J·K$^{-1}$·mol$^{-1}$) | $\Delta G^\circ$ (kJ·mol$^{-1}$) |
|---|---|---|---|---|
| Kao | 298 | −37.77882 | −149.57 | 6.79304 |
| | 313 | | | 9.03659 |
| | 323 | | | 10.53229 |
| | 333 | | | 12.02799 |
| Na-MMT | 298 | 85.45961 | 268.71 | −5.38403 |
| | 313 | | | −1.3538 |
| | 323 | | | − 1.33372 |
| | 333 | | | − 4.02082 |
| F13 | 298 | −50.73203 | −172.93 | 0.80111 |
| | 313 | | | 3.39539 |
| | 323 | | | 5.12436 |
| | 333 | | | 6.85366 |
| F23 | 298 | −21.03442 | −76.29 | 1.70000 |
| | 313 | | | 2.84435 |
| | 323 | | | 3.60725 |
| | 333 | | | 4.37015 |

Table 10 shows the $\Delta G^\circ < 0$ for Na-MMT. This suggests that the mechanism which governes is spontaneous physical adsorption of AO52 and is more favoured at higher temperatures. For Na-MMT, $\Delta H^\circ > 0$: there is endothermic adsorption mechanism.

Conversely, the $\Delta H^\circ < 0$, suggests that the adsorption process is exothermic in nature for Kao, F13 and F23. This shows a physical adsorption process in which

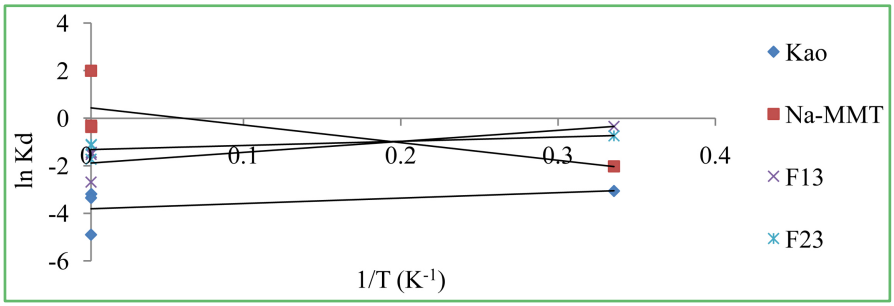


**Figure 18.** Plot of $\ln K_d$ vs $1/T$ for clay materials.

there are Van der Waals attraction [37]. The $\Delta S^{\circ} > 0$ of Na-MMT shows that there is an increase in the disordered on clay materials-dye molecules interface, reflecting the affinity of the adsorbent surface during the adsorption process. Similar result was reported by Ghosh and Bhattaryya [38]. Conversely, for Kao, F13 and F23, the $\Delta S^{\circ} < 0$ shows that there is a random decrease at the interface of adsorbent-solution and during the adsorption process, no change occurs in the inner structure of the adsorbent [39].

## 4. Conclusion

In this study, the natural clays and the two formulations resulting from the calcination of the clay-lime mixture were used to remove CI Acid Orange 52 in aqueous solutions. The results revealed that the calcined clay-lime enhanced the removal capacity and efficiency of CI Acid Orange 52 compared to the natural clay materials. The results also show that in an acid medium, adsorption/coagulation was favourable for the removal of CI Acid Orange 52. In basic conditions, the removal of this dye was favourable by precipitation. F13 and F23 removed over 82% of this acid dye. The physicochemical reaction during the phenomenon involves the adsorption process at the surface of materials and the exchange of ions amid dye and foreign ions in the clay interlayer. Thus, these adsorbents are affordable and sustainable potential adsorbents to remove unwilling organic pollutants such as acid azo-dyes for industrial effluents because of their low cost and availability.

## Data Availability Statement

All data generated or analysed during this study are included in this published article.

## Conflicts of Interest

Authors state no conflict of interest.

## References

[1] Gu, S.Q., *et al.* (2019) Clay Mineral Adsorbents for Heavy Metal Removal from Wastewater: A Review. *Environmental Chemistry Letters*, **17**, 629-654. https://doi.org/10.1007/s10311-018-0813-9

[2] Ravikumar, K., Deebika, B. and Balu, K. (2005) Decolourization of Aqueous Dye Solutions by a Novel Adsorbent: Application of Statistical Designs and Surface Plots for the Optimization and Regression Analysis. *Journal of Hazardous Materials*, **122**, 75-83. https://doi.org/10.1016/j.jhazmat.2005.03.008

[3] Elmoubarki, R., Mahjoubi, F.Z., Tounsadi, H., Moustadra, F.J., Abdennouri, M., Zouhri, A., El Albani, A. and Barka, N. (2015) Adsorption of Textile Dyes on Raw and Decanted Moroccan Clays: Kinetics, Equilibrium and Thermodynamics. *Water Resources and Industry*, **9**, 16-29. https://doi.org/10.1016/j.wri.2014.11.001

[4] Gao, J.F., Zhang, Q., Su, K. and Wang, J.H. (2010) Competitive Biosorption of Yellow 2G and Reactive Brilliant Red K-2G onto Inactive Aerobic Granules: Simultaneous Determination of Two Dyes By First-Order Derivative Spectrophotometry and Isotherm Studies. *Bioresource Technology*, **101**, 5793-5801. https://doi.org/10.1016/j.biortech.2010.02.091

[5] Malik, R., Ramteke, D.S. and Wate, S.R. (2007) Adsorption of Malachite Green on Groundnut Shell Waste Based Powdered Activated Carbon. *Waste Management*, **27**, 1129-1138. https://doi.org/10.1016/j.wasman.2006.06.009

[6] Feng, Y.F., *et al*. (2013) Adsorption of Dyestuff from Aqueous Solutions through Oxalic Acid-Modified Swede Rape Straw: Adsorption Process and Disposal Methodology of Depleted Bioadsorbents. *Bioresource Technology*, **138**, 191-197. https://doi.org/10.1016/j.biortech.2013.03.146

[7] Alorabi, A.Q., *et al*. (2021) Natural Clay as a Low-Cost Adsorbent for Crystal Violet Dye Removal and Antimicrobial Activity. *Nanomaterials*, **11**, Article No. 2789. https://doi.org/10.3390/nano11112789

[8] Vimonses, V., Lei, S., Jin, B., Chow, C.W.K. and Saint, C. (2009) Kinetic Study and Equilibrium Isotherm Analysis of Congo Red Adsorption by Clay Materials. *Chemical Engineering Journal*, **148**, 354-364. https://doi.org/10.1016/j.cej.2008.09.009

[9] Nadiye-Tabbiruka, M.S., Lungani, L., Chaloba, S. and Ddamba, W. (2018) Investigation of Methyl Orange Adsorption from Water Using Acid Activated Makoro Clay. *American Journal of Materials Science*, **8**, 73-78.

[10] Fumba, G., Essomba, J.S., Tagne, G.M., Ndi, J.N., BélibiBélibi, P.D. and Ketcha, J.M. (2014) Equilibrium and Kinetic Studies of Methyl Orange Removal from Aqueous Solutions Using Kaolinite, Metakaolinite and Activated Geopolymer as Low Cost Adsorbents. *Journal of Academia and Industrial Research*, **3**, 156-163.

[11] Serge, E.J., Alla, J.P., Belibi, P.D.B., *et al*. (2019) Clay/Polymer Nanocomposites as Filler Materials for Leather. *Journal of Cleaner Production*, **237**, Article ID: 117837. https://doi.org/10.1016/j.jclepro.2019.117837

[12] Ahmadpour, A., Tahmasbi, M., Bastami, T.R. and Besharati, J.A. (2009) Corrigendum to Rapid Removal of Cobalt Ion from Aqueous Solutions by Almond Green Hull. *Journal of Hazardous Materials*, **166**, 925-930. https://doi.org/10.1016/j.jhazmat.2008.11.103

[13] Mbadcam, J.K., Anagho, S.G., Nsami, J.N. and Kammegne, A.M. (2011) Kinetic and Equilibrium Studies of the Adsorption of Lead(II) Ions from Aqueous Solution onto two Cameroon Clays: Kaolinite and Smectite. *Journal of Environmental Chemistry and Ecotoxicology*, **3**, 290-297.

[14] Shen, D., Fan, J., Zhou, W., Gao, B., Yue, Q. and Kang, Q. (2009) Adsorption Kinetics and Isotherm of Anionic Dyes onto Organo-Bentonite from Single and Multisolute Systems. *Journal of Hazardous Materials*, **172**, 99-107. https://doi.org/10.1016/j.jhazmat.2009.06.139

[15] Foo, K.Y. and Hameed, B. (2010) Insights into the Modelling of Adsorption Iso-

therm Systems. *Chemical Engineering Journal*, **156**, 2-10. https://doi.org/10.1016/j.cej.2009.09.013

[16] Essomba, J.S., Nsami, J.N., BélibiBélibi, P.D., Tagne, G.M. and Mbadcam, J.K. (2014) Adsorption of Cadmium(II) Ions from Aqueous Solution onto Kaolinite and Metakaolinite. *Pure and Applied Chemical Sciences*, **2**, 11-30. https://doi.org/10.12988/pacs.2014.31017

[17] Eloussaief, M., Sdiri, A. and Benzina, M. (2013) Modelling the Adsorption of Mercury onto Natural and Aluminium Pillared Clays. *Environmental Science and Pollution Research*, **20**, 469-479. https://doi.org/10.1007/s11356-012-0874-4

[18] Khan, M.I., Khan, H.U., Azizli, K., *et al*. (2017) The Pyrolysis Kinetics of the Conversion of Malaysian Kaolin to Metakaolin. *Applied Clay Science*, **146**, 152-161. https://doi.org/10.1016/j.clay.2017.05.017

[19] Boulingui, J.E., Nkoumbou, C., Njoya, D., Thomas, F. and Yvon, J. (2015) Characterization of Clays from Mezafe and Mengomo (Ne-Libreville-Gabon) for Potential Uses in Fired Products. *Applied Clay Science*, **115**, 132-144. https://doi.org/10.1016/j.clay.2015.07.029

[20] Chen, D., Chen, J., Luan, X., Ji, H. and Xia, Z. (2011) Characterization of Anion-Cationic Surfactants Modified Montmorillonite and Its Application for the Removal of Methyl Orange. *Chemical Engineering Journal*, **171**, 1150-1158. https://doi.org/10.1016/j.cej.2011.05.013

[21] Vimonses, V., Jin, B. and Christopher, W.K.C. (2010) Insight into Removal Kinetics and Mechanisms of Anionic Dye by Calcination Clay Materials and Lime. *Journal of Hazardous Materials*, **177**, 420-427. https://doi.org/10.1016/j.jhazmat.2009.12.049

[22] Nandi, B.K., Goswami, A. and Purkait, M.K. (2009) Adsorption Characteristics of Brilliant Green Dye on Kaolin. *Journal of Hazardous Materials*, **161**, 387-395. https://doi.org/10.1016/j.jhazmat.2008.03.110

[23] Konan, K.L., Sei, J., Soro, N.S., Oyetola, J.M., Gaillard, J., Bonnet, P. and Kra, G. (2006) Caractérisation des Matériaux Argileux du Site d'Azaguié-Blida (Anyama, Côte d'Ivoire) et Détermination des Propriétés Mécaniques de Produits Céramiques. *Journal de la Société Ouest-Africaine de Chimie*, **21**, 35-43.

[24] Mohammedi, F. (2017) Adsorption des poly organiques en solution aqueuse par des argiles naturelles de la région du Tlemcen. Thèse de Doctorat, Université Abou Bekr Belkaid-Tlemcen-Algérie, Chetouane.

[25] Dal Negro, A., De Pieri, R., Quareni, S. and Taylor, W.H. (1978) The Crystal Structures of Nine K Feldspars from the Adamello Massif (Northern Italy). *Acta Crystallographica*, **B34**, 2699-2707. https://doi.org/10.1107/S056774087800905X

[26] Comodi, P. and Zanazzi, P.F. (2000) Structural Thermal Behaviour of Paragonite and Its Dehydratylate: A High-Temperature Single-Crystal Study. *Physics and Chemistry of Minerals*, **27**, 377-385. https://doi.org/10.1007/s002690000085

[27] Rehman, M.Z.U., Aslam, Z., Shawabkeh, R.A., Hussein, I.A. and Mahmood, N. (2020) Concurrent Adsorption of Cationic and Anionic Dyes from Environmental Water on Amine Fonctionalized Carbon. *Water Science & Technology*, **81**, 466-478. https://doi.org/10.2166/wst.2020.119

[28] Abbas, A., Murtaza, S., Shahid, K., Munir, M., Ayub, A. and Akber, S. (2012) Comparative Study of Adsorptive Removal of Congo Red and Brilliant Green Dyes from Water Using Peanut Shell. *Middle-East Journal of Scientific Research*, **11**, 828-832.

[29] Zhang, X., Hong, H., Li, Z., Guan, J. and Schulz, L. (2009) Removal of Azobenzene from Water by Kaolinite. *Journal of Hazardous Materials*, **170**, 1064-1069.

https://doi.org/10.1016/j.jhazmat.2009.05.073

[30] Adeyemo, A.A., *et al*. (2015) Adsorption of Dyes Using Different Types of Clay: A Review. *Applied Water Science*, **20**, 543-568. https://doi.org/10.1007/s13201-015-0322-y

[31] Saad, S.A., Isa, K.M. and Bahari, R. (2010) Chemically Modified Sugarcane Bagasse as a Potentially Low-Cost Biosorbent for Dye Removal. *Desalination*, **264**, 123-128. https://doi.org/10.1016/j.desal.2010.07.015

[32] Zahir, A., Aslam, Z., Aslam, U., Abdullah, A., Ali, R. and Bello, M.M. (2020) Paspalum Notatum Grass-Waste-Based Adsorbent for Rhodamine B Removal from Polluted Water. *Chemical and Biochemical Engineering Quarterly*, **34**, 93-104. https://doi.org/10.15255/CABEQ.2020.1830

[33] Bulut, E., Özacar, M. and Şengil, I.A. (2008) Equilibrium and Kinetic Data and Process Design for Adsorption of Congo Red onto Bentonite. *Journal of Hazardous Materials*, **154**, 613-622. https://doi.org/10.1016/j.jhazmat.2007.10.071

[34] Li, Y.K., Zhao, B.L., Xiao, W., *et al*. (2013) Kinetic Study of Methyl Orange Adsorption from Solution by IOCZ. *Advanced Materials Research*, **684**, 194-197. https://doi.org/10.4028/www.scientific.net/AMR.684.194

[35] Silva, M.M.F., Oliveira, M.M., Avelino, M.C., Fonseca, M.G., Almeida, R.K.S. and Filho, E.C.S. (2012) Adsorption of an Industrial Anionic Dye by Modified-KSF-Montmorillonite: Evaluation of the Kinetic, Thermodynamic and Equilibrium Data. *Chemical Engineering Journal*, **203**, 259-268. https://doi.org/10.1016/j.cej.2012.07.009

[36] Kumar, M. and Tamilarasan, R. (2013) Modeling of Experimental Data for the Adsorption of Methyl Orange from Aqueous Solution Using a Low Cost Activated Carbon Prepared from Prosopisjuliflora. *Polish Journal of Chemical Technology*, **15**, 29-39. https://doi.org/10.2478/pjct-2013-0021

[37] Kausar, A., Iqbal, M., Javed, A., Aftab, K., Nanzli, Z., Bhatti, H.N. and Nouren, S. (2018) Dyes Adsorption Using Clay and Modified Clay: A Review. *Journal of Molecular Liquids*, **256**, 395-407. https://doi.org/10.1016/j.molliq.2018.02.034

[38] Ghosh, D. and Bhattaryya, K.G. (2002) Adsorption of Methylene Blue on Kaolinite. *Applied Clay Science*, **20**, 295-300. https://doi.org/10.1016/S0169-1317(01)00081-3

[39] Doğan, M., Özdemir, Y. and Alkan, M. (2007) Adsorption Kinetics and Mechanism of Cationic Methyl Violet and Methylene Blue Dyes onto Sepiolite. *Dyes and Pigments*, **75**, 701-713. https://doi.org/10.1016/j.dyepig.2006.07.023